INTERNATIONAL JOURNAL OF
ENERGY RESEARCH

INTERNATIONAL JOURNAL OF ENERGY RESEARCH
Int. J. Energy Res. 2017; **41**:1709–1729
Published online 8 March 2017 in Wiley Online Library (wileyonlinelibrary.com). DOI: 10.1002/er.3734

Nominal energy optimisation method of constrained battery packs through the iteration of the series-parallel topology

Mauricio Fernández-Montoya, Andrés Arias-Rosales*,†, Gilberto Osorio-Gómez and Ricardo Mejía-Gutiérrez

Design Engineering Research Group (GRID), Universidad EAFIT, 050022 Medellín, Colombia

SUMMARY

The design of a battery pack commonly deals with high performance goals and challenging constraints in terms of cost, volume or weight. One of the most crucial variables to maximise is the nominal energy, which depends on the number of discrete battery cells that can be allocated and their individual technical specifications. This work proposes a systematic method to optimise the nominal energy of a constrained battery pack from the perspective of the series-parallel topology. A mathematical and graphical characterisation is presented on how the main battery's variables are related to a topology bounded to discretisation procedures. It was theoretically found that the effects of rounding the values of the topology may lead to a considerable loss of potential nominal energy, a risk that increases linearly with the number of series. The behaviour of the battery is assessed under nominal conditions and under the event of a cell failure. The theoretical analysis suggests that the detrimental effects due to an open-circuit increase as the number of series increases, while it is the opposite in the case of a shorted cell. The method is satisfactorily implemented in the development of two different battery packs for solar competition cars with limiting regulations. The candidate topologies outperformed the nominal energy of topologies defined without the method in up to 5%. It was also found that selecting an energy-maximising topology is not always the most convenient choice, because other variables may be of interest and are dependent on the topology as well. The method is of great use to guide the topology definition process in early theoretical stages, which is usually a compromise between allocating as much cells as possible within constraints, and approaching other performance goals such as a given nominal voltage or capacity. Copyright © 2017 John Wiley & Sons, Ltd.

KEY WORDS

battery; series-parallel topology; optimisation; solar car; cell failure

Correspondence

*Andrés Arias-Rosales, Design Engineering Research Group (GRID), Universidad EAFIT, 050022 Medellín, Colombia.
†E-mail: aariasr@eafit.edu.co

Received 10 September 2016; Revised 26 January 2017; Accepted 27 January 2017

1. INTRODUCTION

There is currently a global trend towards broadening the implementation of electrical technologies for industrial and domestic applications. When their energy demand cannot be entirely generated in the same place of consumption, it is necessary to store the energy so it can be readily available. Electrochemical battery packs offer a way of delivering electric energy on demand after transforming the potential energy stored in chemicals [1]. However, battery packs for electrical devices, especially the portable ones, must usually comply with strict practical limitations, which in turn constrains the energy output. While battery cells keep improving their energy density [2], electrical systems keep increasing their energy demand in the quest for extended performance. This scenario underscores the need for optimising the nominal energy output of constrained battery packs.

Numerous optimisation methods of battery pack performance can be found in literature: the chemistry and electrodes within the cells [3]; the thermal management systems and strategies [4–6]; the electrical cell balancing [7–9]; the reduction of resistance and leakage among connections [7]; and the assessment of the effects of the series-parallel topology. With 'topology', this work refers to the electrical structure with which the individual battery cells are interconnected; a concept also found in literature as the layout of the battery pack [10]. The electrical structure of the topology can be defined in terms of the number of series, the number of parallels and the way in which the cells are grouped in modules. As Plett and Klein [11] state, when the number of individual cells is numerous, they are

arranged in modules for technical practicality. When these modules are connected in series, while the cells within are connected in parallel, they are known as 'parallel cell modules' (PCM). Conversely, if the modules are connected in parallel, with the cells within connected in series, the configuration is known as 'series cell modules' (SCM). The *capacity of the battery pack* (C_{BP} [*Ah*]) rises as the *number of parallels* (*nP*) increases. Similarly, the *pack's nominal voltage* (V_{BP} [*V*]) rises with the *number of series* (*nS*).

The series-parallel topology is commonly regarded merely as a means to achieve a minimum requirement of voltage, capacity or power [4,5,12–18]. The number of parallels *nP* and series *nS* of a battery pack is normally calculated directly by applying the laws of Kirchhoff and Ohm [19]. *nS* could be calculated from both the objective voltage V_{BP} and the *cells' nominal voltage* (V_{BC} [*V*]). Having a *pack's power* objective (P_{BP} [*W*]) and an *autonomy* objective (*t* [*h*]), the needed capacity C_{BP} would then be known. Subsequently, it would be possible to directly calculate the required number of parallels *nP*. Baronti *et al.* [20] provide an example of a direct topology definition process based on the capacity and voltage requirements. Nevertheless, they conveniently choose objective values for the pack that are multiples of the characteristics of the cells, and thus, they avoid considering the rounding-discretisation effects.

The previously described procedure, that is, directly calculating *nS* and *nP* from the laws of Kirchhoff and Ohm, results in real numbers, as opposed to integers. Therefore, *nS* and *nP* would have to be rounded-up or rounded-down to the next whole number. This discretisation process may lead to unwanted implications, such as exceeding a *maximum number of allowable battery cells* (nBC_{max}) according to the general constraints. A direct rounding procedure may also lead to topologies incapable of satisfying the pack's specification objectives or which do not take full advantage of the available ranges. Not considering the discretisation effects in that process may undermine the capacity to take full advantage of the allowable constraining ranges, leading to a 'nominal energy loss', that is, when a theoretical nominal energy margin is left unused due to a discretisation process in the topology definition.

This is a critical issue when optimising a battery pack, because that wasted margin could otherwise be used to further increase the energy output. For instance, if from weight restrictions 100 battery cells would be allowed, but the number of series is defined as 45, then the maximum number of parallels would be 2 within weight constraints. This would mean a nominal energy loss of 10 cells, that is, 10% less energy than what could have been theoretically achieved while still respecting the general boundaries. This work illustrates how addressing the nominal energy loss due to a discrete topology can get to a more complex design scenario, where several candidate topologies must be carefully compared and more variables should be considered in early design stages.

Based on the limitations and risks described, regarding the topology definition, it is reasonable to propose the series-parallel topology itself as an optimisation perspective. Xue *et al.* [10] developed a method to optimise a battery pack for a hybrid vehicle from the internal characteristics of the cells and their series-parallel topology. However, they implemented a highly specific and computationally demanding algorithm and did not address in detail the implications of discretisation. Similarly, the work of Sakti *et al.* [21] included certain aspects of the battery pack's topology within an optimisation process, but the connections among and within modules were all assumed to be in series without further flexibility. In the work of Song *et al.* [22], a hybrid battery/super-capacitor system is examined for optimisation in a process where the series-parallel topology is iterated, but its discrete implications were not characterised in detail. In a further work, Song *et al.* [23] defined a minimum number of cells for a battery pack but then adjusted that number without a systematic approach into one which was allegedly 'appropriate for grouping', namely, that could be achieved through a discrete topology. The latter illustrates how the discretisation procedures, concerning the battery topology, are commonly performed in a straightforward manner without a deeper exploration of their effects over the pack's nominal characteristics or without a detailed comparison among the range of possible topology candidates.

Several authors addressed, directly or indirectly, the implications of a battery pack's topology over variables of key interest. Plett and Klein [11] discussed advantages and disadvantages of the topology configurations PCM and SCM, considering the impact over the pack's longevity, the tolerance towards cell failure, the ability to self-correct and the complexity for cell management and monitoring. Similarly, Song *et al.* [22] characterised the capacity loss depending on the series-parallel topology. On the other hand, Chiu *et al.* [24] analysed the thermal implications, such as capacity fade, contrasting between cells connected in parallel and in series. In addition, Lamb *et al.* [26] studied the thermal runaway propagation in different series-parallel topologies.

Another crucial consideration regarding the topology of a battery pack is the behaviour when a cell fails, switching to an open-circuit (OC) or short-circuit (SC) state. By no means is it appropriate to keep using a battery pack while one or more of the cells are known to be failing. However, it is worth assessing the pack's behaviour when such situations arise in order to develop the capacity to identify when and how a pack is failing. Also, under certain circumstances, it might not be possible to detect the failure of a single cell so the battery could unknowingly remain in use under failure conditions. Gholami *et al.* [25] studied battery pack topologies based on their failure tolerance. Plett and Klein [11] assessed the behaviour towards cell failure comparing SCM and PCM arrangements. Several authors assessed the effects of SCs and OCs focusing on different series-parallel topologies [16,26–29].

Int. J. Energy Res. 2017; **41**:1709–1729 © 2017 John Wiley & Sons, Ltd.
DOI: 10.1002/er

From the performed literature review, it can be underscored that several key variables have been analysed in relation to the series-parallel topology of a battery pack. However, very few consider the topology itself as a means for optimisation and, the ones who do, merely include the topology within an iterative optimisation algorithm without further discussion on the topic. No detailed characterisation was found regarding the exposed discretisation effects and risks. Nor was it found an analysis of how a discrete topology may be related to the behaviour of the battery when a cell is in SC or OC.

Addressing this knowledge gap, this work proposes a systematic method to optimise the nominal energy output of a constrained battery pack from the perspective of a topology bounded to discrete values. By describing the development of the method, and through the case study implementation, this work provides a mathematical and graphical characterisation of how the main battery's variables are related to a discrete topology under constraints. In addition, phenomena such as the risk of nominal energy loss are examined in order to derive general equations. To the best of the author's knowledge, there is no battery optimisation method found in the literature with the same perspective as the one proposed in this work, nor is it found such a characterisation of the discretisation processes in topology definition. Furthermore, the detailed case study may serve as a reference for similar implementations. Accordingly, this work is a contribution to the state of the art and can be complemented in further design stages with other published methods for broadening the battery pack optimisation perspectives.

2. OPTIMISATION METHOD FOR BATTERY PACK TOPOLOGIES

This section describes a method developed to optimise the nominal energy of constrained battery packs from the perspective of a topology bounded to discretisation processes. As the objective is towards nominal energy, the healthy battery cells are assumed to work under nominal conditions and with no imbalances among them. The only situation in which the pack is evaluated for non-nominal behaviour is when one cell turns into a SC or an OC. In this situation, the other cells that are not directly affected are assumed to work under nominal specifications. It is hence worth stating that the mathematical model presented along the method is not intended for a realistic simulation of a real battery pack under use but for a first-stage optimisation based on nominal behaviours and on specific cell faults, that is, OC or SC. This work can serve as a useful tool to define battery pack topology candidates, which may then be examined by considering other variables that are beyond the focus of this method, such as the ageing effects, manufacture imbalances or temperature implications [30].

The main steps of the method are summarised in Figure 1 and are described in detail throughout this section. The method starts by defining the technical guidelines in terms of the constraints and performance objectives. After a portfolio of possible battery cells is defined, every cell is analysed for all the discrete topologies which are allowable within constraints. This numerical analysis comprises the impact over the nominal energy output and the main pack's specifications; both under nominal and failure conditions. Afterwards, the suitable topologies are graphically compared, and the series-parallel layout, as well as the cell reference, are defined.

2.1. Definition of the technical guidelines and battery cell portfolio

Electrochemical batteries are continuously improving their performance but are still not competitive in terms of energy density, as opposed to gasoline for instance [10]. This scenario, combined with high-energy demanding applications, often leads to battery packs that are too heavy, bulky or costly to be practical.

As shown in Figure 1, Step 1 of the method is to define the technical guidelines for the battery pack. This consists in stating the limiting boundaries and the performance objectives. The users of the method must consider if there are relevant constraints regarding the *weight of the battery pack* (W_{BP} [kg]), the *pack's volume* (VOL_{BP} [m^3]), the *pack's cost* (CO_{BP} [USD]), the *minimum nominal voltage* (V_{BPmin} [V]) and the *maximum nominal voltage* (V_{BPmax} [V]). These were the constraints that were found to be more common, but the users may state any other relevant variables considered to directly limit the battery pack according to the specific implementation. Similarly, the users may consider some of the proposed constraints as irrelevant for their application. For instance, a cost constraint may not be relevant for a competition vehicle, or a weight constraint may not be limiting for a stationary implementation.

To define the pack's nominal voltage limits, the specifications of the peripheral devices that are directly related to the battery are considered. Two direct boundaries are then established, that is, the lower output boundary V_{min} and the upper output boundary V_{max}. As a precaution, a *proportional safety margin sm* is defined. These limits must not be exceeded by the pack at any time. Therefore, it should also be considered that, along the discharge curve, the voltage of the cells ranges from a *maximum cell's voltage* mV_{BC} to a minimum *cut-off voltage* coV_{BC}. Equations (1) and (2) consider such behaviour within the redefinition of the limits in function of the pack's nominal voltage.

$$V_{BPmin} = V_{min}*(1+sm)*\frac{V_{BC}}{coV_{BC}} \quad (1)$$

$$V_{BPmax} = V_{max}*(1-sm)*\frac{V_{BC}}{mV_{BC}} \quad (2)$$

As part of the technical guidelines, it is crucial to define the performance objectives expected from the battery pack. Even though the power needed may vary in time, it is

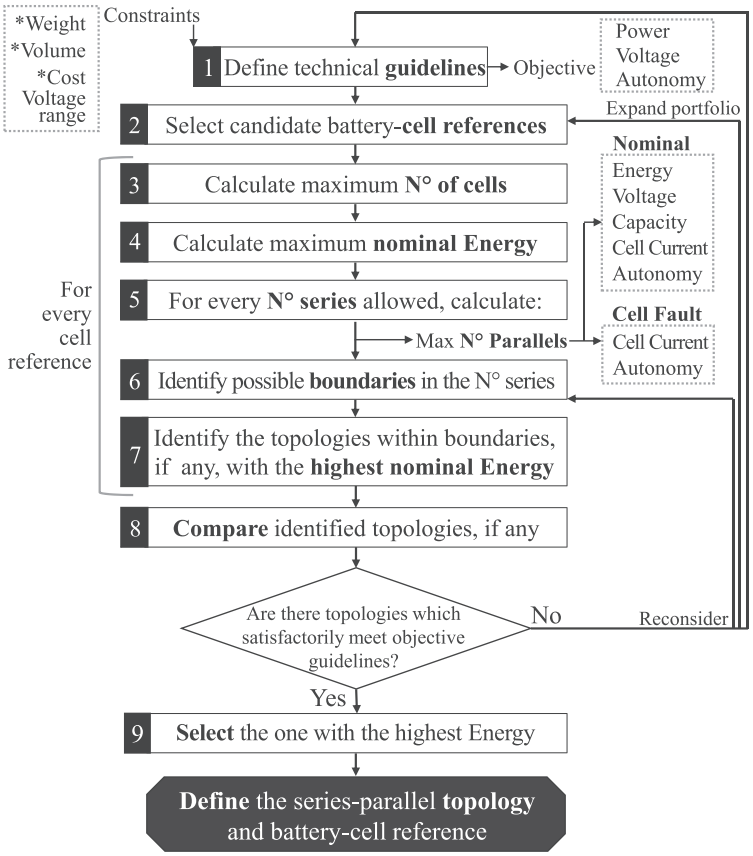

Figure 1. Flow chart of the proposed optimisation method for battery pack topologies.

suggested for the user to define an average nominal situation for design purposes in which a constant power P_{BP} is wanted at a nominal voltage V_{BP} with a minimum t autonomy.

Guided by the technical guidelines, it is then possible to perform Step 2 of the method, a selection of candidate battery cells. The method suggest to first define one or several battery types, according to the constraints and power specifications, and then select specific commercial battery cell references. Saw *et al.* [7] compared different battery types and show lithium-ion batteries as the most appealing in terms of specific energy [$Whkg^{-1}$], specific power [Wkg^{-1}], efficiency and life cycle. However, lithium-ion batteries present disadvantages in terms of cost, safety and environmental hazard. For high-performance systems with highly restrictive constraints of weight and/or volume, lithium-ion batteries may result as the best choice. By contrast, when the most challenging constraint is the capital cost, lead-acid or NiCd batteries may be more viable.

For each reference of the selected candidate battery cells, it is suggested to determine the nominal voltage (V_{BC}), the maximum cell's voltage (mV_{BC}), the cut-off cell's voltage (coV_{BC}), the *cell's capacity* (C_{BC} [Ah]), the *maximum current that can be safely drained from the cell* (I_{BCmax} [A]) at the maximum continuous C-rate, the *cell's weight* (W_{BC} [kg]), the *cell's cost* (CO_{BC} [USD]) and the *volume occupied by the cell* (VOL_{BC} [m^3]).

2.2. Delimitation of the allowable range of topologies

As the main objective is to optimise the nominal energy output, it is a direct priority to maximise nBC_{max}. Equation (3) defines nBC_{max}, which must be calculated for every candidate battery cell reference; Step 3 of the method. The effect of the battery cells being discrete units is addressed in Eq. (3) with the math symbol $\lfloor\rfloor$, which means that the result of the expression inside must be rounded-down to the next integer. The symbol (*) is used in Figure 1 to underscore the variables that can directly limit nBC_{max}.

$$nBC_{max} = min\left\lfloor \left(\frac{W_{BP}}{W_{BC}+W_{ex}}\right), \left(\frac{CO_{BP}}{CO_{BC}+CO_{ex}}\right), \left(\frac{VOL_{BP}}{VOL_{BC}+VOL_{ex}}\right)\right\rfloor \quad (3)$$

Battery cells inside a battery pack imply more elements than just the cells themselves, such as connectors, sensors, supporting structures or empty spaces between them for cooling purposes. Regarding these extra elements, W_{ex} refers to their weight, CO_{ex} refers to their cost

Int. J. Energy Res. 2017; **41**:1709–1729 © 2017 John Wiley & Sons, Ltd.
DOI: 10.1002/er

and VOL_{ex} refers to their volume. nBC_{max} can be taken as an upper limit for the maximum number of battery cells given specific constraints. Correspondingly, a *maximum energy* (E_{BPmax} [Wh]) can be calculated with Eq. (4). E_{BPmax} is the nominal energy that could be produced if all nBC_{max} cells were to be allocated in the pack. Step 4 of the method consists in calculating E_{BPmax} for all the references selected in Step 2.

$$E_{BPmax} = nBC_{max} * V_{BC} * C_{BC} \tag{4}$$

The real *discrete number of battery cells* (nBC) that can in fact be placed in the battery pack may not reach E_{BPmax}, because nBC depends on a *discrete number of series* (nS_R) and a *discrete number of parallels* (nP_R), as stated in Eq. (5).

$$nBC = nS_R * nP_R, \text{ where } (nS_R, nP_R) \in \mathbb{N} \tag{5}$$

As neither the number of series nor the number of parallels can be less than 0, it is possible to determine that the range of both variables is $[1, nBC_{max}]$.

2.3. Numerical calculations

Given a discrete number of series, it is possible to calculate the corresponding *maximum number of discrete parallels* (nP_{Rmax}) with Eq. (6). This equation accounts for the effect of nP_R being an integer with the '$\lfloor\ \rfloor$' symbol shown. The whole range of maximising series-parallel couples can be defined when nP_{Rmax} is calculated for every possible number of series throughout $[1, nBC_{max}]$. For the numerical calculations of Step 5 of the method, all the variables are defined in function of the number of series, taking into account that every number of series is coupled with its corresponding nP_{Rmax}. It is worth mentioning that these equations could have been defined in function of the number of parallels instead. The authors arbitrarily chose nS_R as the independent variable because it was found that a method based on nP_R would converge in the same topology conclusions. Such symmetry results evident in Figure 4(b).

$$nP_{Rmax} = \left\lfloor \frac{nBC_{max}}{nS_R} \right\rfloor \tag{6}$$

For every candidate battery cell, the following calculations must be performed throughout the whole allowable range of nS_R with equations derived from the laws of Kirchhoff and Ohm [19]. The equations are defined in function of input variables from Steps 1 and 2 and nS_R in such a way that the series-parallel couples are maximised without exceeding the constraints stated in Step 1. Equation (7) defines the nominal energy (E_{BP} [Wh]) that can be obtained from a series-parallel maximising couple. The focus of this method is to maximise E_{BP} from a discrete topology. This maximisation is performed numerically because E_{BP} is a discrete function and hence, it cannot be derived for a direct optimisation. Equation (8) calculates the pack's nominal voltage V_{BP}. Equation (9) calculates the pack's capacity C_{BP}. Equation (10) defines the *current that must be drained from each battery cell* (I_{BC} [A]) to sustain a total power P_{BP}. Equation (11) defines the autonomy t for a constant P_{BP}.

$$E_{BP} = nS_R * V_{BC} * C_{BC} * \left\lfloor \frac{nBC_{max}}{nS_R} \right\rfloor \tag{7}$$

$$V_{BP} = V_{BC} * nS_R \tag{8}$$

$$C_{BP} = C_{BC} * \left\lfloor \frac{nBC_{max}}{nS_R} \right\rfloor \tag{9}$$

$$I_{BC} = \frac{P_{BP}}{V_{BC} * nS_R * \left\lfloor \frac{nBC_{max}}{nS_R} \right\rfloor} \tag{10}$$

$$t = \frac{V_{BC} * C_{BC} * nS_R}{P_{BP}} * \left\lfloor \frac{nBC_{max}}{nS_R} \right\rfloor \tag{11}$$

The series-parallel topology also affects the battery pack's behaviour towards failure. In this work, there are two kinds of faults assessed: an OC and a SC in one of the cells. The failure analysis of this work is in agreement with what was found on literature [11,16,26–29].

When an OC takes place in a PCM configuration, the module where the failing cell is located loses a branch of the parallels within it. In order to keep delivering the same current as the other healthy modules, the failing module must increase the current drained from each of its battery cells within. As those cells would be discharging at a higher C-rate, the failing module would have a reduced autonomy, limiting the autonomy of the whole battery pack. However, V_{BP} is not expected to get directly affected in nominal terms.

In the case of an OC taking place in an SCM configuration, the entire failing module would get effectively disconnected from the rest of the battery pack. This happens because the series within the failing module is interrupted. Similarly as with a PCM configuration, the current drained from the remaining battery cells would have to increase in order to maintain the same total current output. This in turn reduces the autonomy of the battery pack for a given P_{BP}. The previous phenomenon occurs because, in an SCM configuration, every module is a branch of the parallel comprising the whole battery pack, and therefore, an OC would cause the main parallel to lose a branch. As with a PCM, the nominal V_{BP} is not expected to get affected. The difference between both configurations is that with SCM, the current uniformly increases in all the remaining battery cells, whereas with a PCM configuration, it only increases in the remaining cells of the failing module. However, the net effect over autonomy is expected to be approximately the same, and the battery cells for which the current is increased suffer an approximately equal

increment for both configurations. Equation (12) defines the *current that must be drained from the remaining battery cells after an OC* (I_{BCOC} [A]) in order to maintain the same P_{BP}. Equation (13) can be used to approximate the new *battery pack's autonomy in the case of an OC* (t_{OC} [h]).

$$I_{BCOC} = \frac{P_{BP}}{V_{BC}{*}nS_R{*}\left(\left\lfloor\frac{nBC_{max}}{nS_R}\right\rfloor - 1\right)} \tag{12}$$

$$t_{OC} = \frac{V_{BC}{*}C_{BC}{*}nS_R}{P_{BP}}{*}\left(\left\lfloor\frac{nBC_{max}}{nS_R}\right\rfloor - 1\right) \tag{13}$$

When an OC happens, the performance of the battery pack is compromised, but it is expected to remain useful in most cases. However, if such situation is identified, an immediate intervention and suspension of use is highly recommended to prevent further damage and underuse of the battery pack.

On the other hand, when a SC takes place without extra electrical protections, the consequences can render the battery pack useless. It is certainly dangerous to keep using a battery pack in the case of a shorted cell. Therefore, it is not of interest for this work to estimate the pack's performance under such conditions within a design method. However, the SC fault is assessed seeking to explore the impact of the series-parallel topology over the high currents that are expected to arise within the pack. The individual cells are modelled as voltage sources with a nominal V_{BC} and an *internal resistance* R_{BC}. Other more precise cell models are found in literature, such as the one proposed by Oh *et al.* [31], but the representation used in this work serves as a useful tool for the purposes of the method. For this analysis, the internal resistances of the cells should not be neglected, because they play a considerable role in limiting the currents within the pack during a SC. Additionally, no external loads are considered for these simplified scenarios.

When a SC happens in a PCM configuration, the *current flowing towards the failing SC cell* (I_{SC} [A]) can be analysed by first isolating the failing module. As there is no external load, no current should be flowing from the other unaffected modules. The healthy cells within the failing module can then be grouped into an equivalent battery as stated by the Thevenin's theorem [32]. This Thevenin-equivalent battery is then shorted and I_{SC} can be defined from Ohm's law. After the Thevenin's equivalent voltage and equivalent resistance are defined, I_{SC} can be stated in function of the number of series with Eq. (14). The energy from the remaining battery cells in the failing module would be drained into the SC until the whole failing module gets completely discharged or until a thermal runaway happens. This in turn interrupts the series connections between modules. Hence, the battery pack cannot keep being used even though the other healthy modules may still have energy in their battery cells.

$$I_{SC} = \left(\left\lfloor\frac{nBC_{max}}{nS_R}\right\rfloor - 1\right)\frac{V_{BC}}{R_{BC}} \tag{14}$$

From Eq. (14), it can be seen that when $nS_R = nBC_{max}$, there is only one parallel, and therefore, it indicates that all the cells are connected in series and $I_{sc} = 0A$ is correctly predicted as expected. Also, when $nS_R = 1$, it indicates a pack configuration of only one module with all the cells connected in parallel.

When a SC occurs in an SCM configuration, the possible outcome depends on several factors and the impact over the overall performance is not entirely straightforward. A SC would not immediately affect the capacity of the battery pack, but it reduces the voltage of the failing module. As those modules are connected in parallel, they cannot have different voltages according to Kirchhoff's laws. It is hence expected for the other healthy modules to start passing current towards the failing module. In this process, the voltage of the modules could reach an intermediate equilibrium or the difference in voltage could be so considerable that the other modules could get completely discharged. As the internal resistance of the battery cells is usually relatively low, the flow of current towards the failing module could be dangerously high, leading to possible overheating, thermal runaway and battery pack failure.

In order to calculate an expected I_{SC} in an SCM configuration, the cells from the healthy modules are first grouped into a Thevenin's equivalent battery. Afterwards, Ohm's and Kirchhoff's voltage laws are implemented with corresponding Thevenin's equivalent voltage and resistance. Lastly, I_{SC} can be stated in function of the number of series with Eq. (15).

$$I_{SC} = \left(\left\lfloor\frac{nBC_{max}}{nS_R}\right\rfloor - 1\right){*}\frac{V_{BC}}{R_{BC}\left(\left\lfloor\frac{nBC_{max}}{nS_R}\right\rfloor(nS_R - 1) + 1\right)} \tag{15}$$

From Eq. (15), as previously discussed for the case of PCM, when $nS_R = nBC_{max}$, there is only one parallel and $I_{sc} = 0A$ is correctly predicted. When $nS_R = 1$, all the cells are connected in parallel and the equation converges into Eq. (14).

Step 5 of the method is fulfilled by solving Eqs 6–15 throughout the allowable range of nS_R for every candidate cell reference.

2.4. Identification of the boundaries within delimited ranges

When performing the calculations enlisted in Section 2.3, it is ensured that the battery pack is not exceeding the constraints marked with (*) in Figure 1. This is because those constraints are directly used in the calculation of nBC_{max}. However, there are other constraints bounded to the battery

pack's topology that may still be exceeded, that is, I_{BCmax}, V_{BPmin} and V_{BPmax}. Depending on the objectives regarding fault resistance, it should also be considered if I_{BCmax} could be exceeded in the case of an OC or if there would be a complete battery pack failure in that situation. Therefore, as stated in Step 6 of the method (Figure 1), further boundaries should be calculated, if possible, in function of nS_R in order to take into account a broader impact of the series-parallel topology.

Seeking to delimit a range in nS_R that respects V_{BPmin} and V_{BPmax}, Eqs (16) and (17) define the low (nS_{RL}) and high (nS_{RH}) boundaries, respectively. It should be noted that nS_{RL} is rounded-up, while nS_{RH} is rounded-down to the next integer.

$$nS_{RL} = \left\lceil \frac{V_{BPmin}}{V_{BC}} \right\rceil \tag{16}$$

$$nS_{RH} = \left\lfloor \frac{V_{BPmax}}{V_{BC}} \right\rfloor \tag{17}$$

In order to ensure that I_{BC} and/or that I_{BCOC} do not exceed the safety limit I_{BCmax}, it might be possible to set further boundaries in the number of series. Equations (10) and (12) define the current that must be drained from the battery cells to sustain P_{BP}, under normal conditions or in the event of an OC, respectively. These equations cannot be analytically solved for nS_R because of their discrete nature. However, as Eqs (10) and (12) are to be solved in Step 5 for all the allowable series-parallel couples, it is possible to directly identify if there are cases where I_{BCmax} is exceeded. If so, it would be possible to set further boundaries in the range of nS_R.

In the event of an OC, it was identified that a total battery pack failure would occur if there is only one parallel in the topology; Eq. (18) defines this situation. Similarly as with I_{BCmax} limit, it is possible to identify when the equality of Eq. (18) is satisfied while inspecting the numerical results from Step 5.

$$1 = \left\lfloor \frac{nBC_{max}}{nS_R} \right\rfloor \tag{18}$$

On the other hand, the maximum power that can be obtained from the battery pack without exceeding I_{BCmax} can be estimated. Equation (19) calculates the maximum power in nominal conditions (P_{BPmax} [W]), while Eq. (20) does so for the event of an OC ($P_{BPOCmax}$ [W]).

$$P_{BPmax} = V_{BC} * I_{BCmax} * nS_R \left\lfloor \frac{nBC_{max}}{nS_R} \right\rfloor \tag{19}$$

$$P_{BPOCmax} = V_{BC} * I_{BCmax} * nS_R \left(\left\lfloor \frac{nBC_{max}}{nS_R} \right\rfloor - 1 \right) \tag{20}$$

2.5. Selection of the battery pack's topology

Step 7 identifies the topologies of highest interest. To facilitate this process, the method proposes to plot a graph of E_{BP} in function of nS_R and graphically mark the boundaries identified, as can be illustrated in the case study presented in Section 3. This process should be performed for every candidate battery cell reference, and if there are series-parallel topologies that respect the boundaries, the ones with the highest E_{BP} should be identified as the candidate topologies for selection.

For Step 8 of the method, the topologies identified as candidate topologies are compared in detail by considering as much information as possible besides the energy output. Table I describes the way in which this work proposes to perform such comparison. With three graphs vertically aligned, each one with two Y axis, it is possible to compare the topologies in terms of the impact of the series-parallel topology. The proposed way of considering the boundaries for this comparison is by marking the forbidden ranges in nS_R with shadowed areas. The allowable range in nS_R would then consist of the areas where no shadows are present. A graphical implementation of these guidelines is presented in the case study (Section 3).

I_{SC} is not included in Table I because the authors believe that the risk of a SC should be principally addressed with additional safety devices, such as intermediate fuses. Therefore, I_{SC} is not a decisive variable for the topology definition. However, it could be optionally included in Graph 3 for Y axis 1 (Table I). Otherwise, the I_{SC} behaviour could be analysed after the topology has been defined for additional safety considerations.

The method supports a highly informed assessment by delivering the whole panorama of topology options for every battery cell reference. By carefully analysing the implications over the response variables, the user can identify the topologies that satisfactorily meet the guidelines and that respect the boundaries with a sufficient margin. As stated in Step 9 of the proposed method, the next step is to select the candidate topology with the highest E_{BP}. Therefore, the selection can then be completed by choosing the series-parallel topology and the battery cell reference.

As indicated in Figure 1, it is possible that none of the series-parallel topologies satisfactorily meet the guidelines

Table I. Description of the proposed comparison of topologies through three graphs.

	Graph 1	Graph 2	Graph 3
X axis	nS_R	nS_R	nS_R
Y axis1	Energy [Wh]	Capacity [Ah]	Current [A]
Variables	E_{BP}, E_{BPmax}	C_{BP}	I_{BC}, I_{BCOC}
Y axis2	N^o parallels	Voltage [V]	Autonomy [h]
Variables	nP_{Rmax}	V_{BP}	t, t_{OC}

and boundaries. Several such contradictory situations of interest are described below:

1. Constraints are too limiting: If one or more of the constraints W_{BP}, VOL_{BP} or CO_{BP} is too low, the maximum number of cells nBC_{max} could be too low as well. This situation could undermine the fulfilment of one or more of the objectives stated in the technical guidelines. In terms of autonomy, it may happen that the maximum achievable t, sustaining a power P_{BP}, is less than the minimum autonomy expected. The objective power itself may be unachievable ($P_{BPmax} < P_{BP}$) or the maximum reachable voltage could be less than the minimum ($V_{BP} < V_{BPmin}$, with $nS_R = nBC_{max}$). Under this scenario, the recommended procedure would be to first expand the portfolio of candidate battery cells in accordance with the most challenging constraint. On the other hand, the user could reconsider the technical guidelines seeking a more realistic technical brief.
2. The battery cell current is too high: The current needed to be drained from each battery cell exceeds the safety maximum current ($I_{BC} > I_{BCmax}$). If all the calculated topologies exceed this limit, it may be necessary to expand the battery cell portfolio, widen the constraints or reduce the power objective. Even if there are some topologies that respect I_{BCmax}, the contradictory situation may still arise if the voltage boundaries (nS_{RL} and nS_{RH}) overlap. Figure 2(a) illustrates such scenario; with shadowed areas indicating the range in nS_R where a boundary is exceeded. As can be seen, there is no nS_R free of shadowed areas, because the ranges where I_{BCmax} is respected do not match the range within the voltage limits. In such a situation, the user may directly consider different voltage specifications for the battery pack or follow the previously described options, such as expanding the battery cell portfolio.
3. The voltage boundaries make the energy maximum peaks unfeasible: As illustrated in Figure 2(b), the unshadowed range in nS_R, which delimits the allowable range, may not match a good enough option in terms of E_{BP}. Such a scenario would keep the user from choosing a near global or local maximum (marked with circles in the graph) in the E_{BP} curve, which means that the energy could not be maximised for that battery cell reference. In this situation, the user could accept the allowable topology with the highest E_{BP} or reconsider the battery cell portfolio and guidelines looking for a further energy maximisation closer to E_{BPmax}.
4. The battery cell current is too high when OC happens: Figure 2(c) presents a scenario where I_{BC} does not exceed I_{BCmax} but I_{BCOC} does. If the allowable range due to this situation does not match the allowable range within voltage boundaries, there may not be any satisfactory topology. If a topology gets selected within the allowable voltage range, the user could reduce the power demand up to $P_{BPOCmax}$ in order to keep the current under safe boundaries even in the case of an OC. The user may also reconsider the voltage specifications in order to select a safer topology in the case of OC without limiting P_{BP}.
5. The allowable range may imply a fatal failure when OC happens: As stated in Eq. (18), there may be a fatal battery pack failure when OC occurs if $nP_R = 1$. Figure 2(d) illustrates a situation where the user may be forced to select a topology because of voltage restrictions and with which that fatal failure could happen. As this situation could be too risky, the user should reconsider the technical guidelines or expand the battery cell portfolio.

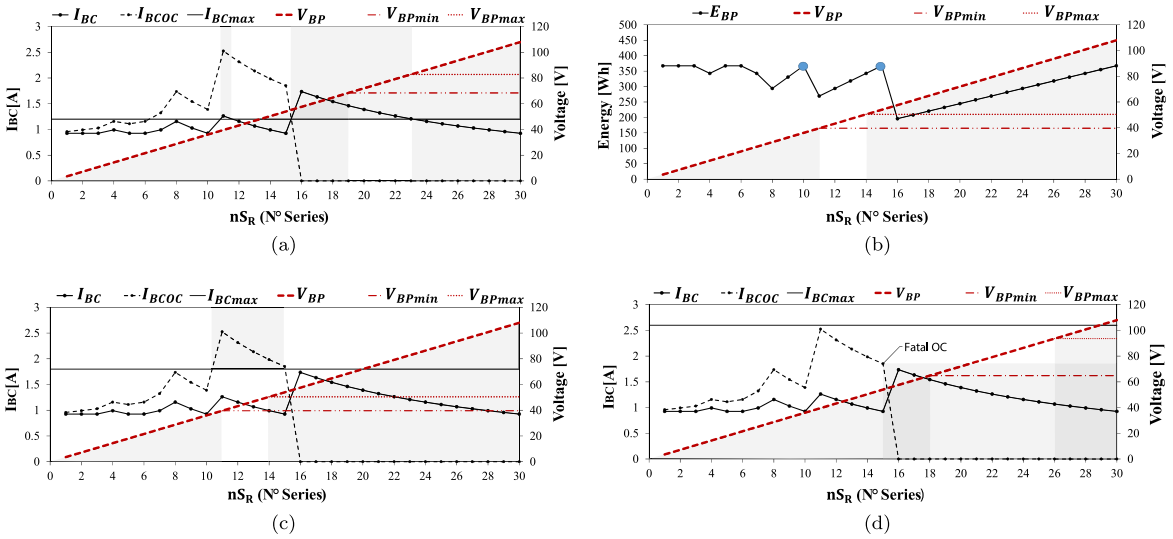

Figure 2. Contradictory situations where no topology is satisfactory. (a) The cell current exceeds the safety maximum. (b) The voltage boundaries imply a too low energy. (c) The cell current is too high when open-circuit (OC) happens. (d) Fatal failure when OC happens. [Colour figure can be viewed at wileyonlinelibrary.com]

3. IMPLEMENTATION OF THE METHOD

In order to explore the implications of the method, and seeking to assess its practicality for supporting the topology definition process, the method is implemented in two successive case studies: Solar competition cars developed to compete in the 'World Solar Challenge' (WSC). A solar car is an electric vehicle that harvests energy from the sun with a photovoltaic array. The obtained power from the array is stored in a battery pack, which ultimately supplies the energy for the electric motors propelling the vehicle. The solar competition cars are selected as the application for the case studies because they offer a challenging scenario where battery packs are strictly constrained, the energy and efficiency demands are high and the voltage specifications are carefully defined.

Even though solar competition cars are not yet intended for practical purposes in commercial applications, they serve as a platform to develop new technologies, improve engineering methods and spread the interest towards clean energy solutions. For these reasons, several events around the world encourage the solar car competitions, with the WSC being one of the most renowned and influential. In this event, solar cars from all over the world participate with the goal to drive from the city of Darwin to the city of Adelaide, Australia. This journey must be completed on a single initial charge of the battery pack, which receives power throughout the competition only from the solar array and a regenerative braking system [33]. Seeking to push the limits further with these events, in each WSC, the organisers restrict more the allowable solar harvesting area and the battery pack's constraints. With such highly competitive conditions, it is of great interest to optimise the energy that can be stored in the vehicle's battery pack while respecting the regulatory constraints.

The case studies of this work revolve around the 'Primavera' solar car project, which has already served as a convenient platform for testing new engineering approaches and methods for research purposes [34–36]. The project is divided into two phases, that is, 'Primavera 1' and 'Primavera 2'. *Primavera 1* is known as the first solar car designed and built in Colombia. It competed in the WSC 2013 and managed to travel for 2505 km. *Primavera 2* competed in the WSC 2015 and managed to complete the whole race by its own means (with solar power and an initial full charge of the battery), travelling 3022 km towards the finish line. The comparison of both phases offers the opportunity to understand how slight modifications in the technical guidelines can lead to considerably different results in terms of topology definition for a battery pack.

3.1. Definition of the main constraints

Table II presents the regulations for both WSC events in terms of the allowable weight for battery cells according to their chemistry.

Table II. Allowable net weights for battery cells based on their chemistry. Modified from World Solar Challenge 2013 and 2015 regulations [41,42].

Cell chemistry	WSC 2013 (kg)	WSC 2015 (kg)
Li-ion	21.0	20
Li-polymer	22.0	20
LiFePO4	40.0	40
Pb-acid	125.0	125

The battery cell weight regulations of the WSC are designed in such a way that they become the main constraint for nBC_{max}. Because the WSC is a high-performance competition, the cost CO_{BP} is not usually limiting. Also, when lithium is chosen for the battery's chemistry, as most of the current competing teams do, the volume VOL_{BP} is not an issue either because of the relatively high volumetric energy density $[Whm^{-3}]$ of lithium-based cells. For *Primavera 1* and *Primavera 2*, the maximum volume constraints were $0.0594m^3$ and $0.1275m^3$, respectively. Those maximum volumes were calculated from the defined locations of the battery packs within each vehicle, the dimensions of the surrounding systems and their bodyworks. Taking full advantage of the allowable volumes to allocate battery cells would lead to excessive lithium-based weight. Hence, the volume is not considered to be as constraining as the weight is.

In terms of the voltage limitations, it is crucial to consider the specifications of the electrical devices related to the drive-train. The maximum voltage of the DC Bus is defined by the minimum upper boundary of the peripheral devices installed in the vehicle. The selected electronic speed controller (*Tritium Wavesculptor22*) can handle a continuous voltage of up to 165 V DC [37]. Therefore, the maximum voltage for the battery pack was defined as $151.8V$, corresponding to the described specifications of the speed controller minus an 8% margin. Similarly, the minimum voltage constraint was defined as $43.2V$, corresponding to the boundary specifications of the selected maximum power point tracker plus an 8% margin. As both vehicles shared most of the main electrical devices, such as the electronic speed controller, these voltage constraints apply to both *Primavera 1* and *Primavera 2*.

3.2. Battery pack's objectives: theoretical energy model

In order to define the technical objectives of the battery pack, an energy model was developed. Considering that solar vehicles in the WSC usually maintain the same speed for prolonged periods of time with smooth variations, the energy model was centred around estimations of average power consumption. The main forces that the vehicle must overcome with the *force provided by its motors* (F_{Motors}) are the *friction force* (F_f) due to the rolling resistance, the *drag force* (F_D) due to the air resistance and a component of its weight in accordance with the *gradient of the slope*

(*G*). Figure 3(d) presents a free-body diagram where a solar car is analysed considering those forces. Equation (21), modified from [38], can be used to approximate the *power consumption* (P [W]) of both vehicles of the case study while maintaining a *constant speed* ($\overrightarrow{V}$ [ms^{-1}]).

$$P = \frac{\overrightarrow{V}}{n}\left[mg(sin(atan(G)) + cos(atan(G))*C_{rr}) + \frac{1}{2}\rho*C_d*A\left(\overrightarrow{V} - \overrightarrow{V_W}\right)^2\right] \quad (21)$$

Where n is the *power-train efficiency*, m is the *mass of the vehicle* with the passenger included [kg], g is the *gravitational acceleration* [ms^{-2}], C_{rr} is the *rolling resistance coefficient*, ρ is the *air density* [kgm^{-3}], C_d is the *aerodynamic drag resistance coefficient*, A is the *frontal area of the vehicle* [m^2] and $\overrightarrow{V}_W$ is the *wind speed* in the direction of advance [ms^{-1}].

Table III presents the input parameters for the developed models. For every vehicle, there were two model set-ups, that is, a 'Base' model with average conditions and a 'High' model, with more challenging conditions. The Base model was calculated with $\overrightarrow{V}_W = 0ms^{-1}$ and $G = 0$, whereas the High model was defined with $\overrightarrow{V}_W = -5.56ms^{-1}$ and $G = 0.07$; in other words, with a $20kmh^{-1}$ wind speed in the opposite direction of advance and a slope gradient of 7%.

The results of the four calculated models, two scenarios for every car, can be viewed in Figure 3. Figure 3(a) consists in the resulting power consumption, from Eq. (21),

Table III. Input parameters for the energy model of the *Primavera* solar cars for 'Base' and 'High' set-ups.

	Primavera 1	*Primavera 2*
m [kg]	350	282
Design $\overrightarrow{V}$ [ms^{-1}]	27.8	27.8
Wheel ϕ [m]	0.545	0.558
RPM	973.4	950.7
C_dA	0.089	0.0667
C_{rr}	0.00625	0.005
N° motors	2	1
G	0	0
G High	0.07	0.07
$\overrightarrow{V}_W$ [ms^{-1}]	0	0
$\overrightarrow{V}_W$ High [ms^{-1}]	−5.56	−5.56

RPM, revolutions per minute.

in function of the speed of advance. The power consumption curve is shown for the Base and the High modelling scenarios. Also, five points of the graph are highlighted, that is, the consumptions corresponding to the design speed for both *Primavera* vehicles and a consumption point of reference taken from one of the top teams of the event, *Tokai University*. The power consumptions highlighted in Figure 3(a) for the Base model curves were taken as the power objectives (P_{BP}) for each vehicle. Figure 3(b) shows the torque curves per motor for the four models. Even though *Primavera 2* is more efficient than *Primavera 1* in every other aspect, *Primavera 2* presents a higher torque curve due to the fact that it used only one motor. In a second Y axis, Figure 3(b) shows the needed voltage for the motors to reach the revolutions per minute

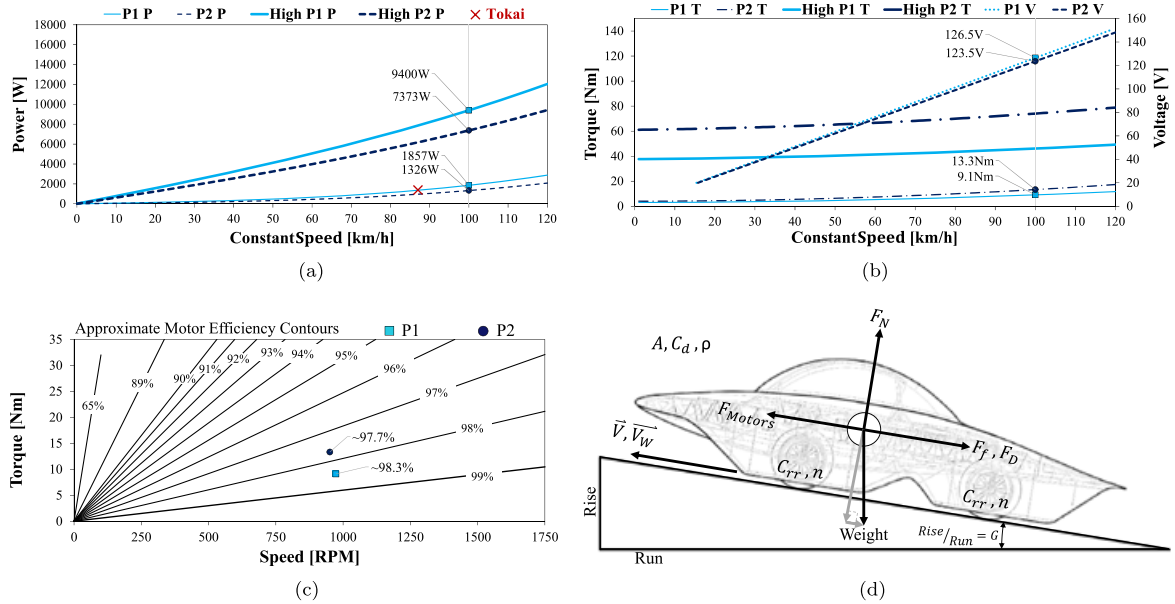

Figure 3. Theoretical energy model of *Primavera 1* (P1) and *Primavera 2* (P2): (a) power consumption; (b) torque per motor and necessary voltage; (c) motor efficiency; and (d) free body diagram. (b) and (c) were developed with information provided by CSIRO manufacturer. RPM, revolutions per minute. [Colour figure can be viewed at wileyonlinelibrary.com]

Int. J. Energy Res. 2017; **41**:1709–1729 © 2017 John Wiley & Sons, Ltd.
DOI: 10.1002/er

[*RPM*] in accordance with the speed of advance in the X axis. Both vehicles differ slightly in the voltage curve because their wheels have different diameters that lead to a different correspondence between the speed of advance and the *RPM* value. From the torque and speed [*RPM*] values, taken from the main Base models, it is possible to estimate the efficiency of the motor; as shown in Figure 3(c). The graphs of the motor's needed Voltage and the motor's efficiency were developed with information provided by the manufacturer *CSIRO*.

The method suggests to define an autonomy (t) objective for the battery pack. However, defining a minimum t is not meaningful for these case studies, and it is considered instead as a variable that is maximised as E_{BP} is maximised.

3.3. Selection of the candidate battery cell references

Considering the technical guidelines defined in Sections 3.1 and 3.2, a portfolio of candidate battery cells is selected. Initially, there were 22 commercial, industrial-use or 'under development' cell references compared. The most competitive ones are described in Table IV and are all based on lithium because of their high specific energy. For instance, while the analysed lithium-ion-based cells have an average specific energy of 180–250 [$Whkg^{-1}$] for commercial references, the lead-acid cells show low specific energy values of 5.5–14 [$Whkg^{-1}$].

The cells from ENVIA Systems and Nomura achieve the highest performance in the general comparisons. However, by the time *Primavera 1* was developed, they were both still experimental [39] or under commercial development. Therefore, for the first vehicle, the battery cells Panasonic NCR18650A and Panasonic NCR8650B are chosen as the main candidates for a detailed topology assessment. On the other hand, the Nomura cells were already available when *Primavera 2* was being developed, and thus, the main candidate references for the second vehicle are the Nomura 8543125SH1 and the Panasonic NCR18650B.

3.4. Analysis of the numerical calculations

As stated in Section 2.3, the numerical calculations start by defining the range of nS_R, which serves as the independent variable for the rest of the calculations:

- *Primavera 1*: nS_R [1,442] for the reference Panasonic NCR18650A (PA1); nS_R [1,432] for the reference Panasonic NCR18650B (PB1).
- *Primavera 2*: nS_R [1,412] for the reference Panasonic NCR18650B (PB2); nS_R [1,240] for the reference Nomura 8543125SH1 (N2).

With Eq. (6), it is then possible to define the maximising series-parallel couples. As an example to illustrate the behaviour of these couples, Figure 4(a) shows nP_{Rmax} in function of nS_R for the selected candidate cells of *Primavera 1*, namely, PA1 and PB1. The dots correspond to the discrete maximising couples, which can be seen in the close-up within the figure. The continuous lines, that is, PA1c and PB1c, correspond to the calculations of nP in disregard of its discrete nature, namely, with continuous functions, which always result in $nS_R * nP = nBC_{max}$. As it is expected, the discrete couples may reach the continuous functions but never exceed them. The farther these dots are to their corresponding continuous function, the more potential nominal energy is lost because less cells could be allocated within constraints. With the intention to assess how well these continuous functions represent their discrete counterparts, their coefficients of determination (R^2) were calculated as 0.9996, 0.9996, 0.9996 and 0.9994 for PA1, PB1, PB2 and N2, respectively. Such high R^2 coefficients illustrate the risk of not carefully considering the discrete nature of the series-parallel topology: Small changes due to rounding up or down may lead to a considerable loss of potential nominal energy.

With the topological exploration of PB1 as an example, Figure 4(b) shows the nominal energy that may be produced for every discrete series-parallel couple within constraints. The upper border of the surface corresponds to the discrete maximising couples described for Figure 4

Table IV. Comparison of the candidate battery cell references for *Primavera 1* (P1) and *Primavera 2* (P2). Units: $\boldsymbol{V_{BC}}$, $\boldsymbol{mV_{BC}}$ and $\boldsymbol{coV_{BC}}$ [V]; $\boldsymbol{C_{BC}}$ [Ah]; $\boldsymbol{W_{BC}}$ [kg]; $\boldsymbol{E_{BPmax}}$ [Wh].

Cell reference	Chem	V_{BC}	mV_{BC}	coV_{BC}	C_{BC}	W_{BC}	P1, nBC_{max}	P1, E_{BPmax}	P2, nBC_{max}	P2, E_{BPmax}
ENVIA Syst.	Li-ion	3.7	4.2	2.5	45	0.365	57	9490.5	54	8991.0
8543125SH1	Li-Po	3.7	4.3	2.75	5.6	0.083	253	5242.2	240	4972.8
NCR18650B	Li-ion	3.6	4.2	2.5	3.2	0.0485	432	4976.6	412	4746.2
NCR18650A	Li-ion	3.6	4.2	2.5	2.9	0.0475	442	4614.5	421	4395.2
Tenergy 18650	Li-ion	3.7	4.2	2.75	2.8	0.048	437	4527.3	416	4309.8
EEMB LIR18650	Li-ion	3.7	4.2	2.75	2.6	0.048	437	4203.9	416	4001.9
UPF476790	Li-ion	3.7	4.2	2.5	3.3	0.061	344	4200.2	327	3992.7
Tenergy 30123	Li-ion	3.7	4.2	2.75	10	0.205	102	3774.0	97	3589.0
UR18650A	Li-ion	3.6	4.2	2.75	2.2	0.043	488	3865.0	465	3682.8

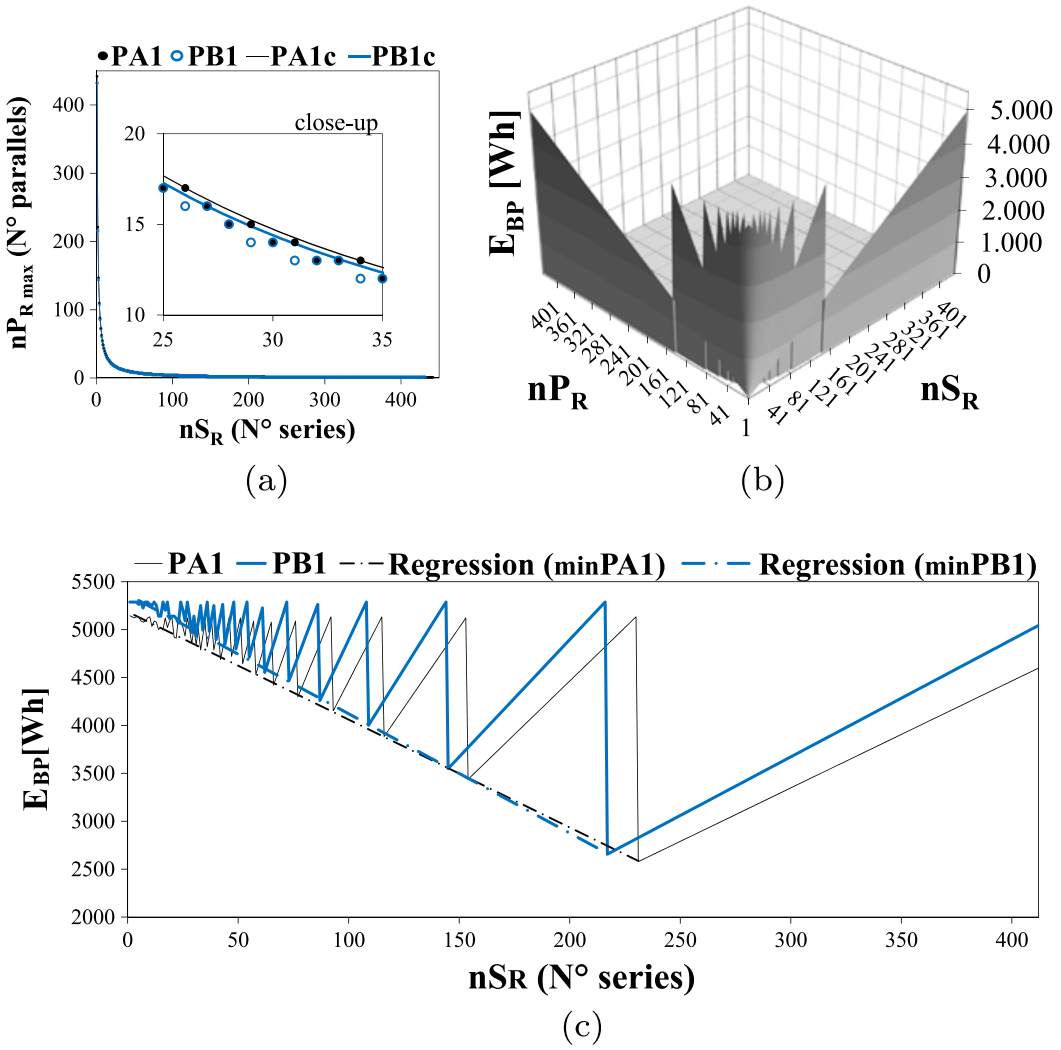

Figure 4. Analysis of the numerical behaviour. (a) Maximising series-parallel couples. (b) Nominal energy achievable by the series-parallel couples for PB1. (c) Risk of nominal energy loss. [Colour figure can be viewed at wileyonlinelibrary.com]

(a). The surface ends abruptly after this border because any series-parallel exceeding the border would be in violation of the general constraints, exceeding nBC_{max}. The pronounced Silhouette of this border reveals the considerable differences in nominal energy that may arise even among the maximising couples that are in close proximity. In fact, most of the discrete topologies leading to a high nominal energy peak (local maximums) are directly followed by topologies leading to a valley (local minimums). This can be intuitively understood by identifying the almost vertical lines in the surface's border.

Figure 4(c) shows the nominal energy that could be produced with the discrete maximising couples described in Figure 4(a). The E_{BP} curve is shown in function of nS_R, but it is worth mentioning that E_{BP} is being calculated from nS_R and from the corresponding nP_{Rmax} with Eq. (6). It can be seen that the valleys in the curve grow deeper as nS_R increases. Therefore, the risk of possible nominal energy losses increases as well. For instance, if $nS_R = 48$ were to be defined for PB1, there could be a maximum of 9 parallels, resulting in 432 cells and a nominal energy of 4976.64 Wh. As $nBC_{max} = 432$, the previous topology corresponds to a global maximum. However, if $nS_R = 49$, the maximum number of parallels would be 8 and the number of cells and nominal energy would drop to 392 and 4515.84 Wh, respectively. This slight change in the number of series would mean a nominal energy that is −9.26% less than E_{BPmax}. If the topology were to be defined from $nS_R = 144$ and compared against a topology defined from $nS_R = 145$, the previous effect would be considerably more detrimental: a resulting energy of 3340.8 Wh for $nS_R = 145$; that is, −32.87% less than E_{BPmax}.

With the intention to characterise the previously exposed risk of potential nominal energy loss, linear regressions were performed from the *local minimums of the*

Int. J. Energy Res. 2017; **41**:1709–1729 © 2017 John Wiley & Sons, Ltd.
DOI: 10.1002/er

nominal energy curves ($minE_{BP}$). Equations 22–25 describe $minE_{BP}$ for PA1, PB1, PB2 and N2, respectively.

$$minE_{BP} = -10.678*nS_R + 4683.1, R^2 = 0.9971 \quad (22)$$

$$minE_{BP} = -11.719*nS_R + 5050.7, R^2 = 0.9962 \quad (23)$$

$$minE_{BP} = -11.64*nS_R + 4796.5, R^2 = 0.9977 \quad (24)$$

$$minE_{BP} = -21.095*nS_R + 5081.8, R^2 = 0.9942 \quad (25)$$

By analysing the slopes and intercepts of the previous regressions, Eq. (26) was derived as a general equation applicable to other battery studies. By using this expression for PA1, PB1, PB2 and N2, the R^2 achieved were satisfactorily high: 0.9852, 0.9834, 0.9910 and 0.9699, respectively. The potential nominal energy loss is isolated in Eq. (27) with respect to E_{BPmax}.

$$minE_{BP} = -\left(\frac{E_{BPmax}}{nBC_{max}}\right)*nS_R + E_{BPmax} \quad (26)$$

$$\Delta E_{BPmax} = -\left(\frac{E_{BPmax}}{nBC_{max}}\right)*nS_R \quad (27)$$

Given the risk of potential energy loss, it is of interest to identify the maximum peaks in the E_{BP} curve. In Table V, the number of maximum peaks is identified for the cells of interest, as well as the proportion of those peaks that are local maximums and the average proportional difference between the local maximums and E_{BPmax}, namely the global maximums. It can be seen that there is little proportional difference, on average, between the local and the global maximums. Therefore, the interest in selecting a local maximum increases even when it is not a global maximum as well. This in turn renders the topological exploration more flexible.

With the exploration of PB1 as an example, Figure 5 explores the behaviour of I_{SC} in function of the number of series nS_R and the internal resistance of the cells R_{BC}. The four sub-figures present a close-up of such behaviour to better examine the stepped facets of the surfaces: nS_R is limited to 215, as $I_{SC}=0$ if the series exceed that value; R_{BC} ranges from a plausible [0.01–0.1] Ohms; and I_{SC} is shown below 3000 A for a PCM configuration and below 10 A for a SCM configuration. Figures 5(a) and 5(c) correspondingly show the surfaces for PCM and SCM. The stepped facets arise as a consequence of the discrete topology and they are parallel to the R_{BC} axis. Hence, the borders of such facets reveal how I_{SC} smoothly increases as the internal resistance decreases. On the other hand, Figures 5(b) and (d) correspondingly show slices, of the previous surfaces, which are parallel to the nS_R axis. Therefore, the upper borders of these slices describe the stepped way in which I_{SC} increases as nS_R decreases, for a given internal resistance value.

Table V. Maximum peaks in the E_{BP} curve for the candidate cell references.

Cell ref	N^0 max	Local max (%)	Av ΔE_{BPmax} (%)
PA1	26	69.2	−0.7
PB1	28	28.6	−1.48
PB2	25	76	−1.19
N2	22	9.1	−1.67

With Eqs (10) and (12), it is verified that none of the maximising series-parallel couples, for the four candidate battery cells, surpasses I_{BCmax} in the case of normal operation or even under the event of OC. Therefore, there are no boundaries associated with I_{BCmax}. Nevertheless, there are boundaries in function of nS_R identified in relation with V_{BPmin}, V_{BPmax} and for the case of fatal OC as described in Section 2.4. Figure 6 presents the numerical results for the four candidate battery cell references, two for every vehicle. This figure includes the shadowed areas defined by the calculated boundaries. The regions in the X axis that do not intersect with these greyed areas designate the definitive allowable ranges in nS_R.

3.5. Definition of the battery pack topologies

For every candidate battery cell, there are four topology set-ups selected for a detailed comparison. These set-ups are all within the definitive allowable ranges shown in Figure 6. They are selected among the local maximums (in terms of the E_{BP} curve) and based on the proximity to the voltage objectives defined in Section 3.2. Table VI presents the comparison of these topologies divided by the intended vehicle.

For *Primavera 1*, the selected topology is dPB1, that is, the battery cell Panasonic NCR18650B with 36 series and 12 parallels. dPB1 is chosen because it represents a global maximum in E_{BP}, and it also presents the closest voltage to the objective V_{BP} compared with the other global maximums. The candidate topologies for this battery cell reference are graphically compared in detail in Figure 6(e). The selected topology is calculated to deliver a nominal voltage of 129.6V, which is only a 2.5% higher than the voltage related to the objective speed. With an energy output of 4976.64W, a battery pack with this topology could sustain the objective power P_{BP} for up to 2.68h under nominal conditions and up to 2.457h under the event of an OC. While respecting the maximum discharge current (I_{BCmax}) of the battery cells, the selected topology can still deliver a maximum power of 9953.28W, which is 436% higher than the objective P_{BP} and 5.9% higher than the power needed for the High consumption scenario shown in Figure 3. Under the event of an OC, the battery pack would still be able to deliver up to 9123.84W, which is enough for the Base P_{BP} scenario but would be 2.9% lower than the consumption required for the High scenario. Under nominal power consumption, the battery pack would discharge the battery cells at 1.2A and at 1.3A in the case of OC, which are both safely below I_{BCmax}.

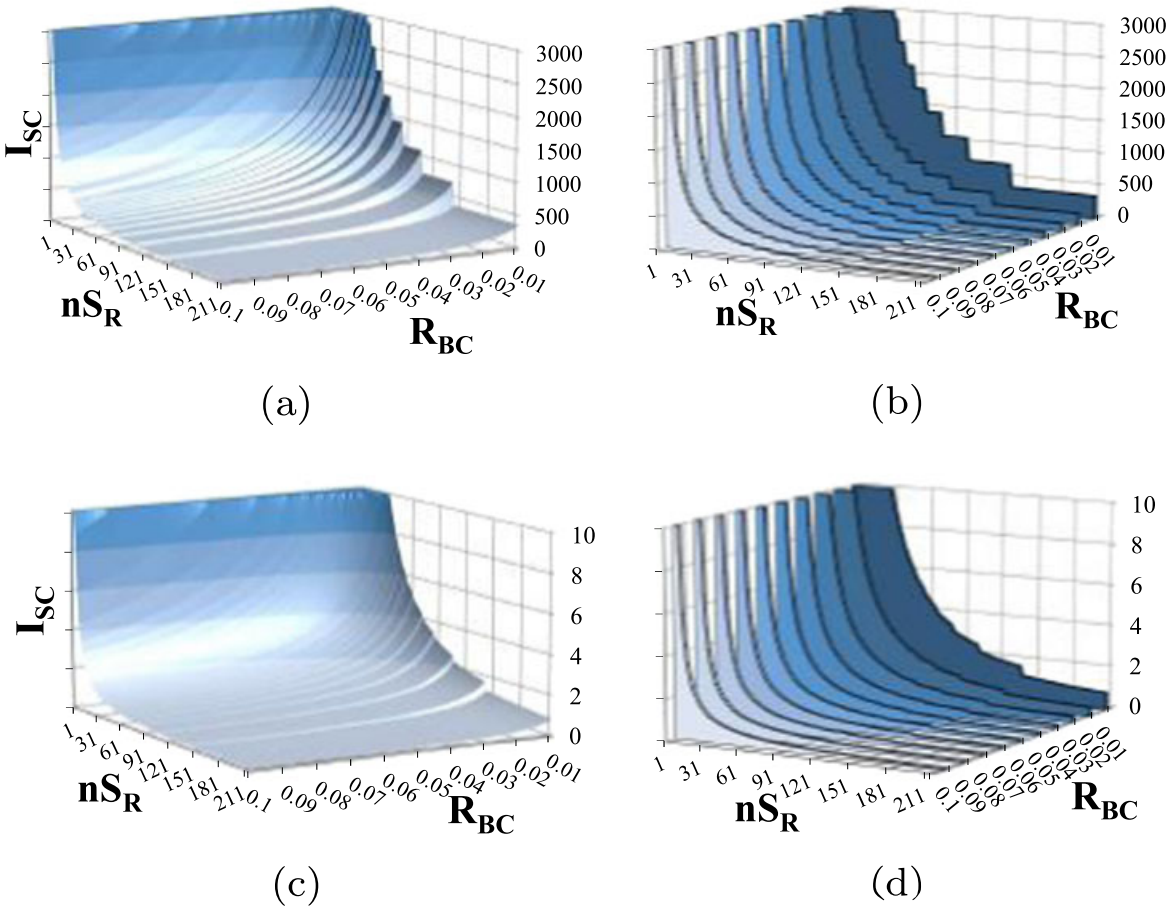

Figure 5. Analysis of the short-circuit behaviour for PB1. (a) and (b) for a parallel cell modules (PCM) configuration; (c) and (d) for a series cell modules (SCM) configuration. [Colour figure can be viewed at wileyonlinelibrary.com]

In the case of *Primavera 2*, the selected topology is dN2, that is, battery cell reference Nomura 8543125SH1 with 34 series and 7 parallels. The candidate topologies for this battery cell reference are compared in Figure 6(f). Even though aN2 and cN2 have an energy output 0.84% higher than the selected topology, they have a nominal voltage that is respectively 28.1% and 10.1% lower than the voltage objective, whereas dN2 has a nominal voltage just 1.9% higher than the objective. Therefore, in this case, it is more convenient to select a local maximum over a global maximum. The set-up dN2 presents an energy output of 4931.36W, which could deliver the objective P_{BP} for 3.72h and 3.19h under OC conditions. The maximum power output is 7397.04W, which is 458% higher than the projected Base consumption and 0.3% higher than the High power consumption scenario. In the event of an OC, the maximum power output is estimated at 6340.3W, which is still 378.2% higher than the Base consumption but 14.0% lower than the High scenario. While sustaining P_{BP} of the Base scenario, $I_{BC} = 1.5A$ and $I_{BCOC} = 1.75A$, which is satisfactory in terms of safety for discharge.

In terms of the SC behaviour of the topology dPB1, I_{SC} is calculated as 720A in PCM or 1.71A in SCM; with an assumed $R_{BC} = 0.055Ohms$ based on [40]. For the topology dN2, I_{SC} is calculated as 2220 A in PCM or 9.57 A in SCM; with an assumed $R_{BC} = 0.01Ohms$ based on information provided by NOMURA CO.

With the intention to challenge the results obtained through the proposed method, the topologies for both vehicles are also calculated in disregard of the discrete topological complexities exposed in this work. The first step is to calculate the number of series nS as the quotient of the objective V_{BP} divided by V_{BC}. nS is then rounded to the next integer to obtain nS_R. The number of parallels nP is calculated as the quotient of nBC_{max} divided by nS_R. Afterwards, nP is rounded up, and down, to the next integers as different candidates. Finally, the nominal performance was calculated for the candidate topologies in which $nBC \leq nBC_{max}$. Table VII presents the results of the previous procedure for the scenarios PA1, PB1, PB2 and N2. In the cases where $nBC > nBC_{max}$, the nominal performance appear as '-' because they would be exceeding the pack's constraints.

In the case of PA1, the nominal energy achieved by the topology that is within constraints is 5% less than the nominal energy achieved by the topology dPA1, which

Int. J. Energy Res. 2017; **41**:1709–1729 © 2017 John Wiley & Sons, Ltd.
DOI: 10.1002/er

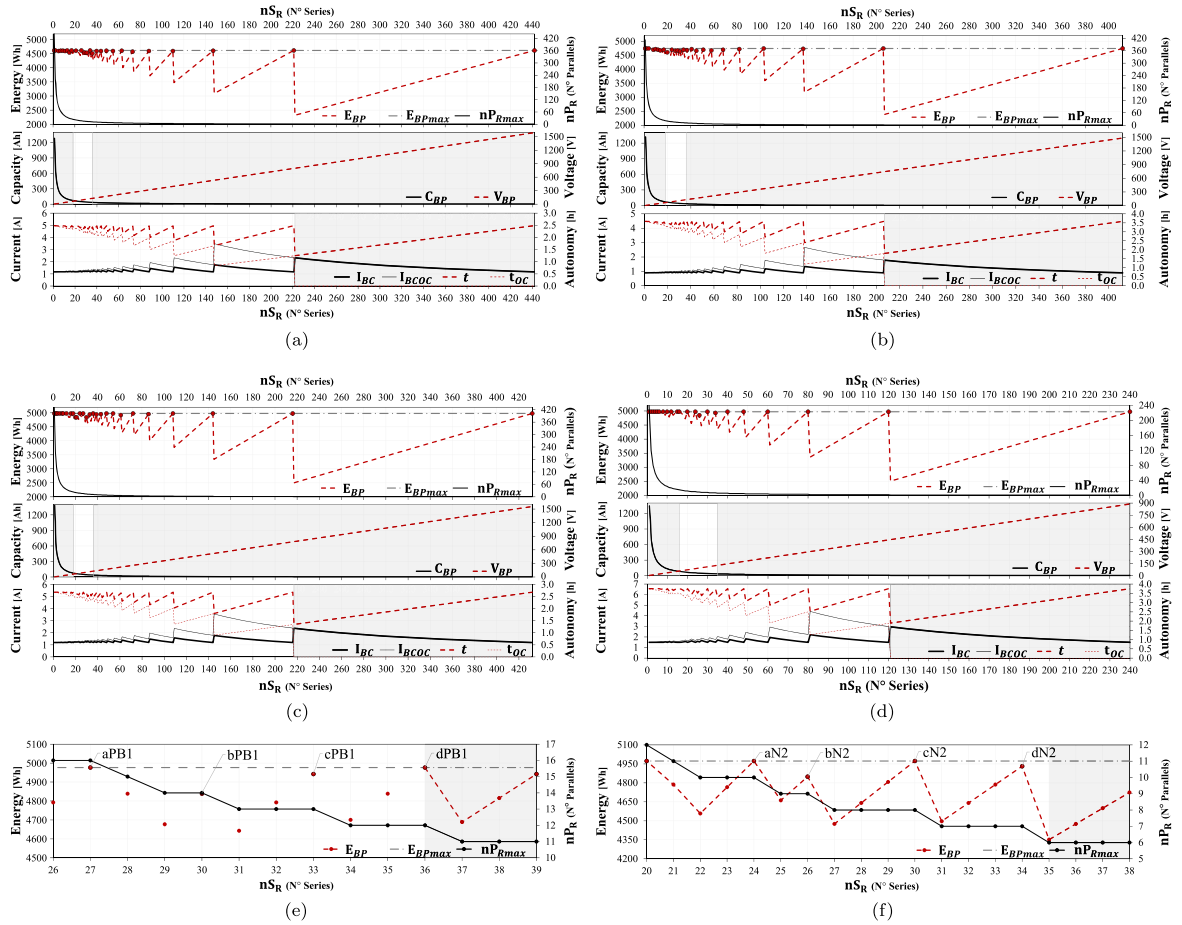

Figure 6. Numerical results of *Primavera 1*: (a) for Panasonic NCR18650A (PA1), (c) for Panasonic NCR18650B (PB1) and (e) a close-up of the latter. Numerical results for *Primavera 2*: (b) for Panasonic NCR18650B (PB2), (d) for Nomura 8543125SH1 (N2) and (f) a close-up of the latter. [Colour figure can be viewed at wileyonlinelibrary.com]

Table VI. Topology set-ups selected to be compared in detail. Units: E_{BP} [*Wh*], V_{BP} [*V*], C_{BP} [*Ah*], I_{BC} and I_{BCOC} [*A*], *t* and t_{OC} [*h*], P_{BPmax} and $P_{BPOCmax}$ [*W*].

Set-up	nS_R	nP_{Rmax}	E_{BP}	V_{BP}	ΔV (%)	C_{BP}	I_{BC}	I_{BCOC}	t	t_{OC}	P_{BPmax}	$P_{BPOCmax}$
aPA1	26	17	4614.5	93.6	−26	49.3	1.167	1.240	2.485	2.339	9229.0	8686.1
bPA1	29	15	4541.4	104.4	−17.5	43.5	1.186	1.270	2.446	2.283	9082.8	8477.3
cPA1	31	14	4531.0	111.6	−11.8	40.6	1.188	1.280	2.440	2.266	9061.9	8414.6
dPA1	34	13	4614.5	122.4	−3.2	37.7	1.167	1.264	2.485	2.294	9229.0	8519.0
aPB1	27	16	4976.6	97.2	−23.2	51.2	1.194	1.273	2.680	2.513	9953.3	9331.2
bPB1	30	14	4838.4	108.0	−14.6	44.8	1.228	1.322	2.606	2.420	9676.8	8985.6
cPB1	33	13	4942.1	118.8	−6.1	41.6	1.202	1.302	2.662	2.457	9884.2	9123.8
dPB1	36	12	4976.6	129.6	2.5	38.4	1.194	1.302	2.680	2.457	9953.3	9123.8
aPB2	27	15	4665.6	97.2	−21.3	48.0	0.909	0.974	3.519	3.285	9331.2	8709.1
bPB2	29	14	4677.1	104.4	−15.5	44.8	0.907	0.977	3.528	3.276	9354.2	8686.1
cPB2	31	13	4642.6	111.6	−9.6	41.6	0.914	0.990	3.502	3.232	9285.1	8570.9
dPB2	34	12	4700.2	122.4	−0.9	38.4	0.903	0.985	3.545	3.250	9400.3	8617.0
aN2	24	10	4972.8	88.8	−28.1	56.0	1.493	1.659	3.751	3.376	7459.2	6713.3
bN2	26	9	4848.5	96.2	−22.1	50.4	1.531	1.723	3.657	3.251	7272.7	6464.6
cN2	30	8	4972.8	111.0	−10.1	44.8	1.493	1.706	3.751	3.282	7459.2	6526.8
dN2	34	7	4931.4	125.8	1.9	39.2	1.506	1.756	3.720	3.188	7397.0	6340.3

Table VII. Topology set-ups calculated without the proposed method. Units: E_{BP} [*Wh*], V_{BP} [*V*], C_{BP} [*Ah*], I_{BC} and I_{BCOC} [*A*], *t* and t_{OC} [*h*], P_{BPmax} and $P_{BPOCmax}$ [*W*].

Set-up	*nS*	nS_R	*nP*	nP_R	E_{BP}	V_{BP}	ΔV (%)	C_{BP}	I_{BC}	I_{BCOC}	*t*	t_{OC}	P_{BPmax}	$P_{BPOCmax}$
PA1	35.14	35	12.63	13	-	-	-	-	-	-	-	-	-	-
	35.14	35	12.63	12	4384.8	126	−0.4	34.8	1.228	1.340	2.362	2.165	8769.6	8038.8
PB1	35.14	35	12.34	13	-	-	-	-	-	-	-	-	-	-
	35.14	35	12.34	12	4838.4	126	−0.4	38.4	1.228	1.340	2.606	2.389	9676.8	8870.4
PB2	34.31	34	12.12	13	-	-	-	-	-	-	-	-	-	-
	34.31	34	12.12	12	4700.2	122.4	−0.9	38.4	0.903	0.985	3.545	3.250	9400.3	8617.0
N2	33.38	33	7.27	8	-	-	-	-	-	-	-	-	-	-
	33.38	33	7.27	7	4786.3	122.1	−1.1	39.2	1.551	1.810	3.610	3.094	7179.5	6153.8

was a global maximum identified by the method in Table VI. In the case of PB1 without the method, the energy achieved within constraints is 2.8% less than the energy achieved by the topology dPB1. For PB2, the topology found without the method matched cPB2, which was the best topology found with the method. Lastly, in the case of N2, the energy achieved within constraints without the method is 2.9% less than the nominal energy of dN2.

After comparing the results in Table VI (from the method) against the results in Table VII (without the method) the topologies dPB1 and dN2 are corroborated as the best topologies for *Primavera 1* and *Primavera 2*, respectively.

3.6. Implementation of the defined topologies

With the cell references selected and the series-parallel topologies defined for both vehicles, the next step is to choose between a PCM or SCM configuration for the sub-modules. Both battery packs are implemented under the PCM structure to simplify and reduce the number of electronic elements needed besides the battery cells. For instance, it is possible to use only one battery management system (BMS) per PCM module, as opposed to one BMS per cell. The simplicity of the vehicle's systems is a priority, because it tends to reduce the possibility of faults in manufacturing, assembly and operation. Moreover, as Baronti *et al.* [20] found for real-life conditions where cells do not always work at nominal specifications, 'the total capacity of SCM is smaller than the total capacity of PCM'. This is because the PCM configuration tends to smooth the possible imbalances that may arise among the cells. As shown in Section 3.5, the selected topologies could potentially present higher I_{SC} for a PCM configuration in the case of a SC. However, this is not taken as a decisive factor for the case study, because the risk of a SC is not addressed from topology but from the implementation of devices such as BMS systems and fuses.

The defined topologies are used as the guidelines to build the two battery packs and implement them in the vehicles *Primavera 1* and *Primavera 2*. Figure 7 presents the physical implementations, with Figures 7(a)–(c) referring to *Primavera 1* and the rest of sub-figures referring to *Primavera 2*.

The discharge response of the real batteries is experimentally measured with the objective to characterise their

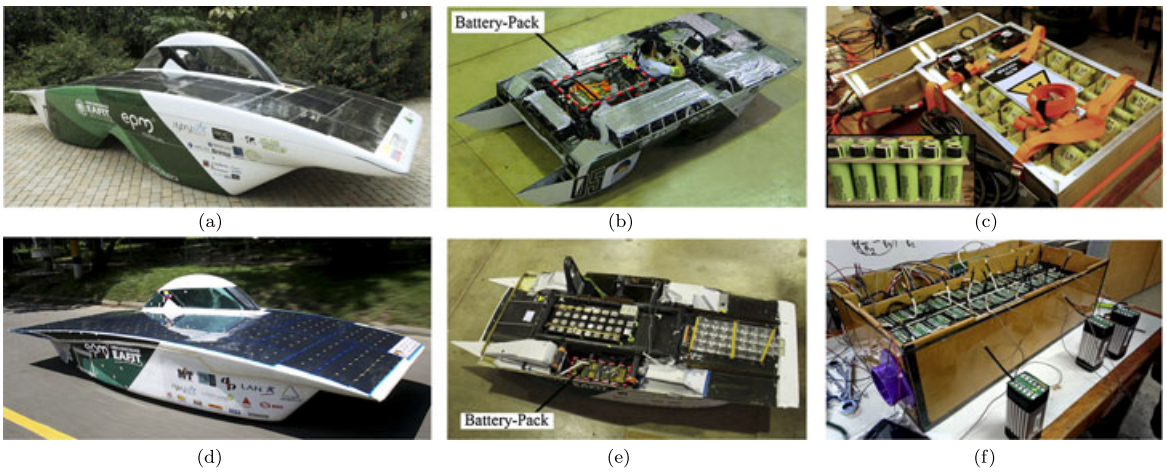

Figure 7. Implementation of the defined topologies. (a) and (d) respectively show the fully functional solar vehicles *Primavera 1* and *Primavera 2*; (b) and (e) respectively show the vehicles with their internal sub-systems exposed, including the battery packs; (c) and (f) present the real functional battery packs with their battery cells and modules visible respectively for *Primavera 1* and *Primavera 2*. [Colour figure can be viewed at wileyonlinelibrary.com]

real behaviour and compare it against the theoretical model and the design constraints. Figure 8(a) shows the discharge curves of the batteries of both vehicles and corresponding polynomial regressions of the fifth order. These curves were first measured from individual cells, that is, a Panasonic NCR18650B and a Nomura 8543125SH1 and then scaled in voltage according to nS_R and in capacity according to nP_R. Based on the real discharge rates of the WSC performed competitions, the battery cell of *Primavera 1* was measured at an average 0.253 C-rate, while the one of *Primavera 2* at 0.157 C-rate. Equations (28) and (29) were obtained from the regressions performed for the batteries of *Primavera 1* and *Primavera 2*, respectively. These equations serve as a continuous characterisation of the discharge voltages in function of the *discharged capacity* (*Dis*). Both regressions present high coefficients of determination (R^2), suggesting that there is a satisfactory fit of the obtained data.

In the case of *Primavera 2*, it was also possible to measure the discharge response directly from the battery pack as a whole, which is shown in Figure 8(b) and defined by Eq. (30). The same was not possible for the complete pack of *Primavera 1* before the WSC competition due to a strategy decision: Such a test could have compromised the extra-charge that the cells may have for their first discharge. The test was performed at an average 0.155 C-rate. There are evident differences between the curves obtained from the pack as a whole compared with the scaled results from a single cell. This may be due to the different measuring equipments and loads used for both tests, given the considerable difference in scale of both experiments. Nevertheless, the energy calculated from both curves closely converges with only a 0.1% difference, as can be seen in Table VIII.

$$V_{BP} = \frac{-7.739Dis^5}{10^6} + \frac{6.484Dis^4}{10^4} - 0.01949Dis^3 + 0.25865Dis^2 - 2.2187Dis + 147.474, \quad R^2 = 0.9913 \tag{28}$$

$$V_{BP} = \frac{-3,541Dis^5}{10^6} + \frac{4,0947Dis^4}{10^4} - 0.01789Dis^3 + 0.3622Dis^2 - 3.828Dis + 138.365, \quad R^2 = 0.9943 \tag{29}$$

$$V_{BP} = \frac{-3.141Dis^5}{10^6} + \frac{3.093Dis^4}{10^4} - 0.01141Dis^3 + 0.19806Dis^2 - 2.23886Dis + 142.737, \quad R^2 = 0.9912 \tag{30}$$

Table VIII presents the main experimental results in

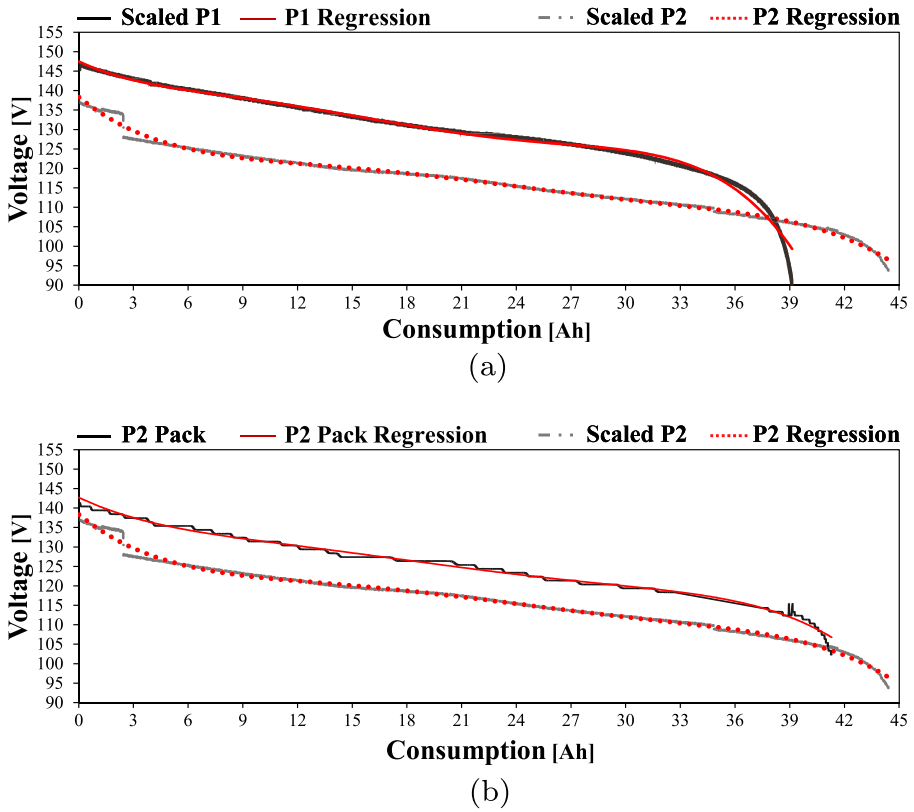

Figure 8. Experimental discharge curves; (a) for both vehicles by scaling individual cell results; (b) for *Primavera 2*, comparing scaled-cell measurements with pack measurements. [Colour figure can be viewed at wileyonlinelibrary.com]

Table VIII. Experimental results compared against theoretical values. Units: E_{BP} [*Wh*], V_{BP} [*V*], C_{BP} [*Ah*], I_{BC} [*A*].

	E_{BP}	Δ (%)	V_{BP}	Δ (%)	V_{BP},max	V_{BP},min	C_{BP}	Δ (%)	I_{BC}	C-rate
P1 theoretical	4976.64		129.60		151.8	43.2	38.40			
P1 experimental scaled	5079.89	2.07	129.15	−0.35	147.02	89.89	39.12	1.88	0.811	0.253
P2 theoretical	4931.36		125.80		151.8	43.2	39.20			
P2 experimental scaled	5162.38	4.68	115.93	−7.84	137.29	93.74	44.41	13.29	0.882	0.157
P2 experimental pack	5156.93	4.57	125.81	0.00	141.44	102.30	41.28	5.31	0.866	0.155

comparison with the theoretical values. The experimental energy output is directly calculated from the measured data with a Riemann sum. In the case of *Primavera 1*, the measured energy is 2.07% more than the theoretical value. Also, the function from Eq. (28) is integrated within the limits of capacity resulting in $E_{BP} = 5080.4Wh$, that is, 0.01% more than the previous result with the Riemann sum. In the case of *Primavera 2*, the experimental energy is 4.68% and 4.57% higher than the theoretical nominal energy, respectively to the scaled cell and whole pack tests. By integrating Eqs (29) and (30), the energy was respectively obtained as 5170 *Wh* and 5163.3*Wh*; both below a 0.25% difference as compared with the corresponding Riemann sums. These results show a close agreement between the nominal energies calculated, the energies obtained from Riemann sums with the experimental data and the areas under the obtained regression functions.

Table VIII also shows a close agreement between the nominal theoretical voltages and the average voltages measured during the discharge of the *Primavera 1* cell and the *Primavera 2* pack. Both batteries respect the voltage theoretical boundaries throughout the discharge curves, as shown by V_{BP},max and V_{BP},min in the table. Furthermore, it is worth mentioning that a board of judges of the WSC satisfactorily approved both batteries and certified that they complied with the tight regulations of the competition.

4. CONCLUSIONS

The topology definition of a battery pack is a trade-off between achieving predefined requirements and maximising the nominal energy by allocating as many cells as possible. The proposed method is of great use in such situations, because it allows a designer/engineer to systematically assess all the possible series-parallel topologies allowed by general boundaries and compare them in terms of key nominal variables, that is, energy, capacity, voltage, maximum power, autonomy and current for a given power. The topologies defined within the case study were theoretically compared against topologies defined without the method, namely, by directly rounding up or down for discretisation. The latter were outperformed by the nominal energies achieved through the method: by 5%, 2.8%, 0% and 2.9% for PA1, PB1, PB2 and N2, respectively.

The maximum number of parallels in function of the number of series is defined by a discrete behaviour that leads to maximising couples. Although this can be approximated with continuous functions with coefficients of determination higher than 0.9994, the small discrepancies between these discrete and continuous functions, due to rounding up or down, may lead to a considerable loss of potential nominal energy. A general equation was derived to describe this behaviour, which implies that the risk of potential nominal energy loss, due to topology definition, increases linearly with the number of series. Furthermore, it was found that most of the discrete topologies leading to a high nominal energy peak (local maximums) are directly followed by topologies leading to a valley (local minimums), which underscores the risk of overlooking the discretisation effects.

It was recognised that there is little proportional difference, on average below 1.7%, between the local and global maximums in nominal energy arising from the series-parallel topology. Therefore, selecting a local maximum may be a feasible compromise to approach objectives in other variables, rendering the topological exploration more flexible. In the case of *Primavera 2*, a local maximum was selected because it closely approached the objective voltage, exceeding it in a 1.9%, while only the 0.83% of the nominal potential energy was not used. On the other hand, the nominal energy of the pack for *Primavera 1* was optimised with a global maximum while complying with all the technical guidelines. Hence, selecting a global maximum in terms of nominal energy, within the allowable range of number of series, is not always the most convenient option overall.

For all the analysed topologies, the cell fault model implies that, if an OC takes place, the cell current needed to be drained for a given power increases with the number of series. Therefore, for higher numbers of series related to less parallels, the risks in the case of an OC are greater. For a single-series array, an OC can lead to a fatal failure of the battery pack. In the case of a shorted cell, high parasitic currents are expected to be drained from the unaffected cells within the pack. The model implies that these currents escalate for a lower internal resistance of the cells and for lower numbers of series.

NOMENCLATURE

Acronyms

BMS = battery management system
N2 = Nomura 8543125SH1 for Primavera 2
OC = open-circuit

Int. J. Energy Res. 2017; **41**:1709–1729 © 2017 John Wiley & Sons, Ltd.
DOI: 10.1002/er

PA1 = Panasonic NCR18650A for Primavera 1
PB1 = Panasonic NCR18650B for Primavera 1
PB2 = Panasonic NCR18650B for Primavera 2
PCM = parallel cell modules
SC = short-circuit
SCM = series cell modules
SOC = state of charge
WSC = World Solar Challenge

Greek Symbols
$\boldsymbol{\rho}$ = air density [kgm^{-3}]

Variables
$\boldsymbol{A}$ = frontal area of the vehicle [m^2]
C_{BC} = capacity of the battery cell [Ah]
C_{BP} = capacity of the battery pack [Ah]
C_d = aerodynamic drag resistance coefficient
C_{rr} = rolling resistance coefficient
CO_{BC} = cost of the battery cell [USD]
CO_{BP} = cost of the battery pack [USD]
CO_{ex} = cost of the supplementary elements besides the battery cell [USD]
coV_{BC} = cut-off voltage [V]
Dis = capacity discharged from a battery pack [Ah]
E_{BPmax} = maximum possible energy within the battery pack's constraints [Wh]
E_{BP} = nominal energy obtainable from a given discrete topology [Wh]
F_D = drag force [N]
F_f = friction force [N]
F_{Motors} = force provided by electric motors [N]
G = gradient of the slope
g = gravitational acceleration [ms^{-2}]
I_{BCmax} = maximum current that can be safely drained from a battery cell [A]
I_{BCOC} = current that must be drained from the remaining battery cells after an OC [A]
I_{BC} = current drained from each battery cell [A]
I_{SC} = current flowing towards a failing module with a cell in short-circuit [A]
m = mass of the vehicle [kg]
$minE_{BP}$ = a local minimum of the energy curve [Wh]
mV_{BC} = maximum cell's voltage [V]
n = power-train efficiency
nBC = discrete number of battery cells
nBC_{max} = maximum number of battery cells within constraints
nP = number of parallels
nP_{Rmax} = maximum number of discrete parallels
nP_R = discrete number of parallels
nS = number of series
nS_{RH} = high boundary in the range of the number of series according to the voltage limits
nS_{RL} = low boundary in the range of the number of series according to the voltage limits
nS_R = discrete number of series
P = power consumption [W]
P_{BPmax} = maximum power that can be safely provided by the battery pack in nominal conditions [W]
$P_{BPOCmax}$ = maximum power that can be safely provided by the battery pack in the event of an OC [W]
P_{BP} = power of the battery pack [W]
R^2 = coefficient of determination
R_{BC} = internal resistance of a battery cell [Ω]
sm = proportional safety margin for voltage limits
t = autonomy [h] of the battery pack for a given power output
t_{OC} = battery pack's autonomy in the case of OC [h]
V_{BC} = nominal voltage of the battery cell [V]
V_{BPmax} = maximum output voltage [V]
V_{BPmin} = minimum output voltage [V]
V_{BP} = nominal voltage of the battery pack [V]
V_{max} = upper output voltage boundary [V]
V_{min} = lower output voltage boundary [V]
VOL_{BC} = volume of the battery cell [m^3]
VOL_{BP} = volume of the battery pack [m^3]
VOL_{ex} = volume of the supplementary elements besides the battery cell [m^3]
$\overrightarrow{V}$ = average speed of the vehicle [ms^{-1}]
$\overrightarrow{V}_W$ = wind speed in the direction of advance [ms^{-1}]
W_{BC} = weight of the battery cell [kg]
W_{BP} = weight of the battery pack [kg]
Wex = Weight of the supplementary elements besides the battery - cell [kg]

ACKNOWLEDGEMENTS

The authors wish to thank Universidad EAFIT and EPM (*Empresas Públicas de Medellín*) as the main sponsors of the project and for all their support and advice provided during the entire solar car project. Also, special thanks to Universidad EAFIT for the postgraduate studies grant 'Undergraduate research excellence scholarship'.

REFERENCES

1. Kousksou T, Bruel P, Jamil A, El Rhafiki T, Zeraouli Y. Energy storage: applications and challenges, USA. *Solar Energy Materials and Solar Cells* 2014; **120**:59–80. doi:10.1016/j.solmat.2013.08.015.
2. Kyriakopoulos GL, Arabatzis G. Electrical energy storage systems in electricity generation: energy policies, innovative technologies, and regulatory regimes, USA. *Renewable and Sustainable Energy Reviews* 2016; **56**:1044–1067. doi:10.1016/j.rser.2015.12.046.
3. Fellner C, Newman J. High-power batteries for use in hybrid vehicles, Lausanne. *Journal of Power Sources*

2000; **85**(2):229–236. doi:10.1016/S0378-7753(99)00344-4.
4. M. Malik, I. Dincer, M. A. Rosen, Review on use of phase change materials in battery thermal management for electric and hybrid electric vehicles, *International Journal of Energy Research* 2016. doi:10.1002/er.3496.
5. Karimi G, Dehghan A. Thermal analysis of high-power lithium-ion battery packs using flow network approach. *International Journal of Energy Research* 2014; **38**(14):1793–1811. doi:10.1002/er.3173.
6. Severino B, Gana F, Palma-Behnke R, Estévez PA, Calderón-Muñoz WR, Orchard ME, Reyes J, Cortés M. Multi-objective optimal design of lithium-ion battery packs based on evolutionary algorithms, Lausanne. *Journal of Power Sources* 2014; **267**:288–299. doi:10.1016/j.jpowsour.2014.05.088.
7. Saw LH, Ye Y, Tay AA. Integration issues of lithium-ion battery into electric vehicles battery pack, Oxford. *Journal of Cleaner Production* 2016. doi:10.1016/j.jclepro.2015.11.011.
8. Kim T, Qiao W, Qu L. Series-connected reconfigurable multicell battery: a novel design towards smart batteries, in: USA. *Energy Conversion Congress and Exposition (ECCE)*2010 IEEE, IEEE 2010:4257–4263. doi:10.1109/ECCE.2010.5617723.
9. Mandal SK, Bhojwani PS, Mohanty SP, Mahapatra RN. Intellbatt: towards smarter battery design, in: USA. *Design Automation Conference*2008. DAC 2008. 45th ACM/IEEE, IEEE 2008:872–877. doi:10.1145/1391469.1391690.
10. Xue N, Du W, Greszler TA, Shyy W, Martins JR. Design of a lithium-ion battery pack for phev using a hybrid optimization method, Sweden. *Applied Energy* 2014; **115**:591–602. doi:10.1016/j.apenergy.2013.10.044.
11. Plett G, Klein M. Simulating battery packs comprising parallel cell modules and series cell modules. In *EVS24 International Battery, Hybrid and Fuel Cell Electric Vehicle Symposium*. European Assn for Battery: Stavanger, Norway, BelgiumHybrid and Fuel Cell Electric Vehicles (AVERE), 2009, 146–163.
12. Y. Wang, L. Li, Li-ion battery dynamics model parameter estimation using datasheets and particle swarm optimization, *International Journal of Energy* 2016. doi:10.1002/er.3497.
13. Cunha Á, Martins J, Rodrigues N, Brito F. Vanadium redox flow batteries: a technology review. *International Journal of Energy Research* 2015; **39**(7):889–918. doi:10.1002/er.3260.
14. Mombeshora ET, Nyamori VO. A review on the use of carbon nanostructured materials in electrochemical capacitors. *International Journal of Energy Research* 2015; **39**(15):1955–1980. doi:10.1002/er.3423.
15. Divya K, Østergaard J. Battery energy storage technology for power systems – an overview. *Electric Power Systems Research* 2009; **79**(4):511–520. doi:10.1016/j.epsr.2008.09.017.
16. Bruen T, Marco J. Modelling and experimental evaluation of parallel connected lithium ion cells for an electric vehicle battery system. *Journal of Power Sources* 2016; **310**:91–101. doi:10.1016/j.jpowsour.2016.01.001.
17. Pendergast DR, DeMauro EP, Fletcher M, Stimson E, Mollendorf JC. A rechargeable lithium-ion battery module for underwater use. *Journal of Power Sources* 2011; **196**(2):793–800. doi:10.1016/j.jpowsour.2010.06.071.
18. J. Jiang, Y. Zhang, W. Shi, J. Xu, W. Diao, H. Guo, An analysis of optimized series and parallel method for traction lithium-ion batteries, in: Intelligent Green Building and Smart Grid (IGBSG), 2014 International Conference on, IEEE, 2014, 1–7.
19. Saslow WM. *Electricity, Magnetism, and Light*. Academic Press, 2002, 336–384.
20. Baronti F, Di Rienzo R, Papazafiropulos N, Roncella R, Saletti R. Investigation of series-parallel connections of multi-module batteries for electrified vehicles. In *Electric Vehicle Conference (IEVC)*2014 IEEE International, IEEE Xplore Digital Library, Piscataway: New Jersey, US. 2014; 1–7.
21. Sakti A, Michalek JJ, Fuchs ER, Whitacre JF. A techno-economic analysis and optimization of li-ion batteries for light-duty passenger vehicle electrification, Lausanne. *Journal of Power Sources* 2015; **273**:966–980. doi:10.1016/j.jpowsour.2014.09.078.
22. Song Z, Li J, Han X, Xu L, Lu L, Ouyang M, Hofmann H. Multi-objective optimization of a semi-active battery/supercapacitor energy storage system for electric vehicles. *Applied Energy* 2014; **135**:212–224. doi:10.1016/j.apenergy.2014.06.087.
23. Song Z, Hofmann H, Li J, Han X, Ouyang M. Optimization for a hybrid energy storage system in electric vehicles using dynamic programing approach. *Applied Energy* 2015; **139**:151–162. doi:10.1016/j.apenergy.2014.11.020.
24. Chiu K-C, Lin C-H, Yeh S-F, Lin Y-H, Huang C-S, Chen K-C. Cycle life analysis of series connected lithium-ion batteries with temperature difference. *Journal of Power Sources* 2014; **263**:75–84. doi:10.1016/j.jpowsour.2014.04.034.
25. Gholami M, Esen H, Schioler H, Stoustrup J. A fault-tolerant control architecture for different battery topologies in electrified vehicles, France. *IFAC Proceedings Volumes* 2012; **45**(20):582–587. doi:10.3182/20120829-3-MX-2028.00251.
26. Lamb J, Orendorff CJ, Steele LAM, Spangler SW. Failure propagation in multi-cell lithium ion batteries.

Journal of Power Sources 2015; **283**:517–523. doi:10.1016/j.jpowsour.2014.10.081.
27. Dubarry M, Devie A, Liaw BY. Cell-balancing currents in parallel strings of a battery system, Lausanne. *Journal of Power Sources* 2016; **321**:36–46. doi:10.1016/j.jpowsour.2016.04.125.
28. Feng Z, Zhang Y. Thermal runaway due to symmetry breaking in parallel-connected battery cells. *International Journal of Energy Research* 2014; **38**(6):813–821. doi:10.1002/er.3086.
29. D. Andrea, Connecting batteries in parallel: unexpected effects and solutions, in: Battery Power Conference 2012, 2012 Available from: http://www.batterypoweronline.com/conferences/2012-conference-pdfs/.
30. Liu X, Chen Z, Zhang C, Wu J. A novel temperature-compensated model for power li-ion batteries with dual-particle-filter state of charge estimation. *Applied Energy* 2014; **123**:263–272.
31. Oh K-Y, Samad NA, Kim Y, Siegel JB, Stefanopoulou AG, Epureanu BI. A novel phenomenological multi-physics model of li-ion battery cells. *Journal of Power Sources* 2016; **326**:447–458.
32. Brittain J. Thevenin's theorem. *Ieee Spectrum* 1990; **27**(3):42.
33. M. S. Group. Available from: http://www.worldsolarchallenge.org/about-wsc-2015/overviewBridgestone world solar challenge overview [online] (2016).
34. Arias-Rosales A, Barrera-Velásquez J, Osorio-Gómez G, Mejía-Gutiérrez R. Designing a concentrating photovoltaic (cpv) system in adjunct with a silicon photovoltaic panel for a solar competition car, in: SPIE Sensing Technology + Applications. *International Society for Optics and Photonics* 2014:91150W–91150W. doi:10.1117/12.2050830.
35. Osorio-Gómez G, Mejía-Gutiérrez R, Suárez-Castañeda N, Gil-Herrera A, Barrera-Velásquez J. Solar array design based on shadow analysis for increasing net energy collection in a competition vehicle, USA. *Journal of Photonics for Energy* 2015; **5**(1):053091–053091. doi:10.1117/1.JPE.5.053091.
36. A. Serrano-Rico, P. Gaviria-Mejía, J. Barrera-Velásquez, G. Osorio-Gómez, R. Mejía-Gutiérrez, Design of a solar competition vehicle strategy with a cyber physical system approach, in Proceedings of the International Virtual Concept Workshop on â€œInnovation on Product Design and Manufacturingâ€. MedellÃn, Colombia.
37. T. P. Ltd. Available from: http://tritium.com.au/wp-content/uploads/2012/07/TRI88.003v2-Datasheet.pdfDatasheet tritium wavesculptor22drive [online].
38. Roche DM. *Speed of Light: The 1996 World Solar Challenge*, Vol. **1**. International Specialized Book Service Incorporated: Australia, 1997, 44–45.
39. E. Systems. Envia high energy density battery cells [online].
40. NASA-JSC. Performance and safety testing of panasonic 2.9 ah li-ion ncr 18650 cells [online] (2009).
41. W. S. Challenge. Available from: http://www.worldsolarchallenge.org/files/7-regulations-for-2013-world-solar-challenge-release-copy-v11.pdfRegulations for the world solar challege 2013 [online].
42. W. S. Challenge. Available from: http://www.worldsolarchallenge.org/files/522-2015-world-solar-challenge-event-regulations.pdfRegulations 2015. world solar challege [online].